

Complex Dark Photon Dark Matter EFT

Enrico Bertuzzo^{a,b,c}, Tomasso Sassi^{d,e}, Andrea Tesi^f

^a*Dipartimento di Scienze Fisiche, Informatiche e Matematiche, Università degli Studi di Modena e Reggio Emilia, Via Campi 213/A, I-41125 Modena, Italy*

^b*INFN sezione di Bologna, via Irnerio 46, 40126 Bologna, Italy*

^c*Instituto de Física, Universidade de São Paulo, C.P. 66.318, 05315-970 São Paulo, Brazil*

^d*Dipartimento di Fisica e Astronomia, Università degli Studi di Padova, Via Marzolo 8, 35131 Padova, Italy*

^e*INFN, Sezione di Padova, Via Marzolo 8, 35131 Padova, Italy*

^f*INFN Sezione di Firenze, Via G. Sansone 1, I-50019 Sesto Fiorentino, Italy*

Abstract

We construct an effective field theory for complex Stueckelberg dark photon dark matter. Such an effective construction can be realized by writing down a complete set of operators up to dimension six built with the complex dark photon and Standard Model fields. Classifying the effective operators, we find that in order to properly take into account the non-renormalizable nature of an interacting massive vector, the size of the Wilson coefficients should be naturally smaller than naively expected. This can be consistently taken into account by a proper power counting, that we suggest. First we apply this to collider bounds on light dark matter, then to direct detection searches by extending the list of non-relativistic operators to include the case of complex vectors. In the former we correctly find scaling limits for small masses, while in the latter we mostly focus on electric dipole interactions, that are the smoking gun of this type of dark matter. Simple UV completions that effectively realize the above scenarios are also outlined.

E-mail: enrico.bertuzzo@unimore.it, tommaso.sassi@phd.unipd.it, andrea.tesi@fi.infn.it

Contents

1	Introduction	2
2	Complex Dark Photon	4
2.1	Symmetry constraints on the effective interactions	5
2.2	Stueckelberg effective field theory	7
3	Structure of the EFT	9
3.1	Power counting possibilities	10
3.2	About the dark photon physical mass	11
4	Matching onto low energy EFT	12
4.1	Matching at the Electro-Weak Scale	12
4.2	Single Nucleon EFT	14
4.3	Non-relativistic Effective Field Theory	15
5	Phenomenological Bounds	17
5.1	Collider Constraints: Higgs and Z invisible decays	17
5.2	Direct Detection	22
5.3	Massless Stueckelberg case	25
6	Sketching possible UV completions	26
6.1	Model I: $SU(2) \times U(1)$	26
6.2	Model II: $SU(2)_L \times SU(2)_R \times \mathbb{Z}_2$	28
7	Conclusions	29
A	Polarizations of massive vectors	30
B	Cross sections for direct detection	32

1 Introduction

The existence of Dark Matter (DM) relies so far just on gravitational evidences, while little is known about its possible non-gravitational interactions (see however [1] for a review). From the particle physics point of view, apart from the obvious absence of strong interactions with us, one of the most remarkable inferred property of DM is its cosmological stability. For ordinary matter, stability arises as a consequence of accidental symmetries of the Standard Model (SM) after all the possible renormalizable interaction terms are written down. Such accidents depend upon the gauge interactions as well as the matter content of the theory. Barring massless particles, as the photons, the stability of electrons and protons are understood in terms of accidental symmetry. In the DM literature the stability is often taken for granted and ensured, for example for phenomenological studies, assuming DM to be (at least) charged under some \mathbb{Z}_2 symmetry, with the SM being a total singlet. Generally speaking, such dark symmetries like \mathbb{Z}_2 can act, so that in these cases it is then possible to study in full generality the effective theory of DM interactions with the SM [2, 3].

In this work, we would like to study effective field theories (EFTs) of DM that are consistent with the idea that DM stability arises accidentally. As such - in analogy to what happens for the SM - we have in mind dark sectors with gauge interactions, where the lightest states are accidentally stable against decay to the SM.

Here we consider DM as a massive vector, a scenario which is commonly known as dark photon, see [4, 5] for reviews. Its simplest realization is characterised by a kinetic mixing interaction with the SM hypercharge. Dark photon can be DM if a \mathbb{Z}_2 symmetry forbids such a kinetic mixing [6–19]. More complicated models involving extensions of the SM with non abelian gauge groups have also been considered, realising stable vector DM candidates by means of renormalisable SU(2) gauge interactions [17, 19–31, 31–33] (see also [34] for an example of confined SU(2)), or larger groups as in [17, 35–37], further generalized to SU(N) in [38–40]. The case in which the dark sector is not a complete singlet under the SM gauge group has been investigated for instance in [41, 42], allowing for electroweak interactions between the two sectors.

Here we focus on a scenario in which dark photon stability arises accidentally, having DM charged under an accidental $U(1)_D$ global symmetry of the dark sector (see *e.g.* [21]), which seems to us the smaller symmetry that can accidentally stabilise the DM. In order to fix the ideas, it is convenient to think about the SM. If we consider a world where there are no fermions, the W^\pm vector bosons will be accidentally stable thanks to a $U(1)$ symmetry (the global rephasing associated to electromagnetism), while the Z boson (or the Higgs) have in principle no right to be stable. Indeed they would decay to W^+W^- if g were sufficiently small. From this very simple ideal example, we are led to consider dark sectors - endowed with dark gauge-Higgs interactions - that deliver dark photons in irreducible representation of $U(1)_D$. Having that in mind, we will remain agnostic about the precise origin of the interactions in the dark sector, excluded for the presence of this $U(1)_D$ accidental symmetry, and only make use of the assumption that the dark matter candidate is a massive complex dark photon that is a complete singlet with respect to SM interactions. We dub these as *complex dark photon* scenarios.

The main purpose of this paper is to consider a bottom-up approach and construct the EFT for complex dark photons stabilized by the accidental $U(1)_D$, for similar studies see [15, 17, 43–50]. We consider M_\star as the effective mass scale of the new sector, while M is the mass of DM, and explore contact interactions between operators constructed with dark photon fields and SM singlet operators. In this context, the interactions between the dark and SM sector are typically casted in terms of a *portal* connecting them, often generated by contact terms of SM singlet fields or carried by some mediator of definite spin. The most studied scenario is that of a scalar portal [6, 8–10, 15, 18, 19, 22, 51], but also models involving a pseudo-scalar [52], a fermion [33, 53] or a vector [36, 54–59] have been considered.

At low energy, DM is described as a Stueckelberg massive vector. While this is a consistent theory when there are no interactions, the presence of interactions between DM and the SM challenges the construction of the EFT. In practice, as we will review below, depending on the strength of the DM-SM interactions, Stueckelberg massive vectors lose perturbativity around a scale $E \gg M$ that can be well below the natural EFT cutoff M_\star . To overcome this problem, in this work we suggest a modified version of the power counting for the size of the Wilson coefficients of our DM EFT that systematically include this effect, by associating to each non-derivative insertion of dark photon fields a suppression proportional to ratio of M/M_\star . This is instrumental to avoid non-physical effects that appear when computing observables with on-shell DM, such as collider bounds.

With the correct power counting, we then explore the direct detection and collider phenomenology (for other works along these lines with somewhat complementary studies, see [21, 46, 51, 58, 60]). We highlight the importance of the Higgs portal even in the dark photon case and we emphasize that

accidentally stable complex dark photon can have - in principle - dipole interactions that give rise to long-range effect in direct detection rates [61]. The latter effect is absent for real dark photons.

The paper is organized as follows. In section 2 we discuss the structure of the operators that can be written down for a complex dark photon, paying attention to redundancies in their definition and to the hidden cut-off inherent to the Stueckelberg nature of the DM. The setup is then applied to identify the leading terms in an EFT expansion in section 3. In section 4 we move to lower energies and match the EFT obtained in the previous section into effective theories valid below the electroweak scale and at the nuclear scale. This matching is instrumental for correctly compute the limits on the Wilson coefficients coming from direct detection experiments. Section 5 constitutes the core of our phenomenological analysis, in which we show the limits on the parameter space coming from direct detection and colliders (focusing, in the later case, on Higgs and Z boson decays), while in section 6 we sketch two possible UV-complete theories that generate, at least in part, our low energy EFT. We draw our conclusions in section 7 and relegate technical material to the appendices.

2 Complex Dark Photon

In this work we consider DM as a complex dark photon, that is a vector field V_μ with a non-trivial complex conjugate \bar{V}_μ , being a total singlet of the SM. The Lagrangian of V_μ is described by the following terms

$$\mathcal{L}_V = -\frac{1}{2}V_{\mu\nu}\bar{V}^{\mu\nu} + M^2V_\mu\bar{V}^\mu + \mathcal{L}_{\text{interactions}}(V_\mu; \text{SM}) . \quad (1)$$

The free part of the above lagrangian displays a global symmetry $U(1)_D$ under which $V_\mu \rightarrow e^{i\alpha}V_\mu$. Such a symmetry, when extended to the full lagrangian, including interactions, acts as a stabilising symmetry for DM, forbidding interactions between one single V and SM fields, all taken to be neutral under $U(1)_D$. Effectively, one can think of this model as if the dark photon V_μ were charged with some dark abelian charge.

At this level, V_μ is a massive Proca field (gauge fixed Stueckelberg vector), described by the generalized Lorenz condition $\partial_\mu V^\mu = 0$, such that it is the solution of a Klein-Gordon equation $(\square + M^2)V_\mu = 0$ with just three physical degrees of freedom. The Fourier modes in momentum- p space are described by three polarization states $\epsilon_\mu^\lambda(p)$ such that $\sum_\lambda \epsilon_\mu^\lambda(p)\epsilon_\nu^{\lambda*}(p) = -g_{\mu\nu} + p_\mu p_\nu/M^2$.

We assume that, at low energies, $U(1)_D$ is a good symmetry of the DM lagrangian. This greatly restricts the interactions between V_μ and the SM fields, allowing us to classify the possible structures arising at low energy in an EFT description. The idea is that at some scale M_\star , new states coupled to V_μ are integrated out. In general, we expect the following structure

$$\mathcal{L} = \mathcal{L}_{\text{SM}} + \frac{1}{M_\star^2}\widehat{\mathcal{L}}_{\text{eff}}(\text{SM}; V_\mu) - \frac{1}{2}V_{\mu\nu}\bar{V}^{\mu\nu} + M^2V_\mu\bar{V}^\mu . \quad (2)$$

At this level, $\widehat{\mathcal{L}}_{\text{eff}}(\text{SM}; V_\mu)$ contains all the interactions between DM and the SM, and we expect it to be a polynomial series in operators of higher dimension. The normalization is such that $\widehat{\mathcal{L}}_{\text{eff}}(\text{SM}; V_\mu)$ has dimension six, but this does not forbid that it can contain operators of any dimensions with the appropriate dimensionful Wilson coefficient. The above structure is meant to render explicit the decoupling limit when the mass scale M_\star is taken arbitrarily large, a limit in which the DM becomes extremely weakly coupled to the SM. Clearly, our EFT is valid up to energies $E \lesssim M_\star$ and can only be applied in this limit.

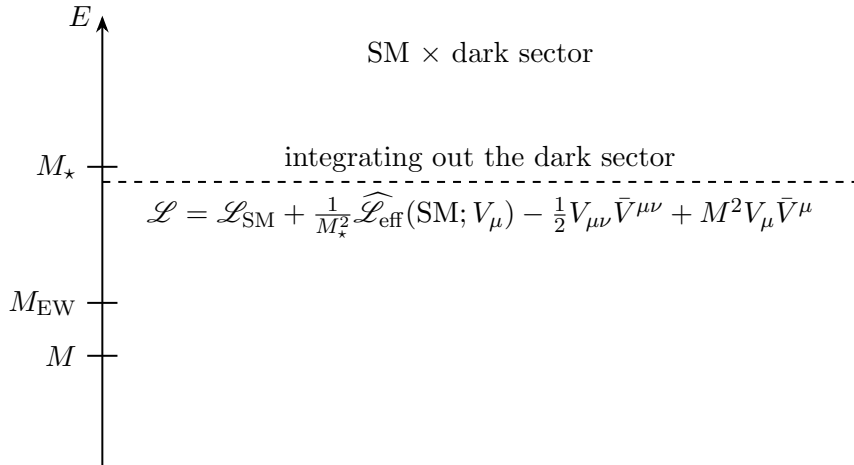


Figure 1. Generation of the DM effective field theory under consideration. We put in evidence the hierarchy of scales needed for the effective description to be valid.

To be included in the EFT, the DM mass must satisfy $M \ll M_\star$, so that all the process important for DM phenomenology can be described within the effective theory. The fundamental theory of which eq. (1) is a low-energy description is depicted in a cartoon in fig. 1. We take the heavy fields that are integrated out to have masses $M_\star \gg M_{\text{EW}}$, with M_{EW} standing for the common mass scale of the heaviest SM states (h, W, t). The matching is then done at a scale M_\star where the SM electroweak symmetry is still unbroken and operators are classified according to SM gauge symmetries.

The systematic construction of the effective field theory coupling the SM and DM, described by $\widehat{\mathcal{L}}_{\text{eff}}(\text{SM}; V_\mu)$, depends on two important assumptions that we now discuss. The first relies on the $U(1)_D$ symmetry to be elevated to full symmetry of the lagrangians in eqs. (1) and (2). The second, instead, relies on the effective description of V_μ as a massive vector field à la Stueckelberg. This implies that eq. (1) is itself an approximate description valid at low energies up to some scale Λ_V . This last point is extremely important, as we can only use the EFT in a correct energy range where $\Lambda_V \gg M_\star$.

2.1 Symmetry constraints on the effective interactions

Since the full theory enjoys $U(1)_D$ but the SM is neutral under such a symmetry, the effective interactions $\widehat{\mathcal{L}}_{\text{eff}}(\text{SM}; V_\mu)$ are constructed with singlets of $U(1)_D$, that necessarily involve at least two powers of V_μ . This forbids for example a kinetic mixing between $V_{\mu\nu}$ and the hyper-charge field strength, which is usually the most dominant effect for the phenomenology of dark photons [4, 20].

We classify the $U(1)_D$ singlet operators in terms of their Lorentz structure. Since we are dealing with a model for DM we only consider operators involving up to two fields V_μ , and up to dimension four. We now discuss in detail the different structures that may appear in the EFT operators, also shown in table 1.

Scalar singlet operators

We first discuss Lorentz scalar operators constructed with V_μ . There are both CP-even and CP-odd singlet operators:

$$\text{scalar : } \mathcal{O}_S = V_\mu \bar{V}^\mu, \quad \mathcal{O}_F = V_{\mu\nu} \bar{V}^{\mu\nu}; \quad \text{pseudoscalar : } \mathcal{O}_P = \epsilon_{\mu\nu\rho\sigma} V^{\mu\nu} \bar{V}^{\rho\sigma}. \quad (3)$$

type	name	expression
scalar	\mathcal{O}_S	$V_\mu \bar{V}^\mu$
scalar	\mathcal{O}_{F^2}	$V_{\mu\nu} \bar{V}^{\mu\nu}$
pseudoscalar	\mathcal{O}_P	$\epsilon_{\mu\nu\rho\sigma} V^{\mu\nu} \bar{V}^{\rho\sigma}$
vector	J_V^μ	$i \bar{V}_\nu \overleftrightarrow{\partial}_\mu V^\nu$
pseudo-vector	J_P^μ	$i \epsilon^{\mu\nu\rho\sigma} \bar{V}_\nu \overleftrightarrow{\partial}_\rho V_\sigma$
symm. tensor	$\mathcal{O}_{\mu\nu}^S$	$V_{(\mu} \bar{V}_{\nu)}$
antisymm. tensor	$\mathcal{O}_{\mu\nu}^A$	$V_{[\mu} \bar{V}_{\nu]}$
traceless stress tensor	$\mathcal{O}_{\mu\nu}^T$	$V_{[\mu\rho} \bar{V}^\rho_{\nu]}$

Table 1. The eight operators constructed with two complex dark photon dark matter fields considered in this work, including up to two derivatives.

Out of these three operators, $\mathcal{O}_S = V_\mu \bar{V}^\mu$ is expected to give the larger effects for phenomenology, since it has the lowest dimensions. Notice also that \mathcal{O}_P could have been added to eq. (1), but being a total derivative does not lead to effects at the perturbative level. As for $V_{\mu\nu} \bar{V}^{\mu\nu}$, it can appear in dimension six operators involving $|H|^2$ affecting, for example, Higgs decay. These operators can then be contracted with the following SM scalar singlet operators

$$\mathcal{O}_{\text{SM}} = \{ |H|^2, |H|^4, F^2, |D_\mu H|^2, \bar{\psi} i \not{D} \psi, QH U, F \tilde{F}, \dots \}. \quad (4)$$

Here $F = G, W, B$ refer to the SM gauge bosons in the unbroken electroweak phase, in agreement with the assumption $M_\star \gg M_{\text{EW}}$. In this paper we follow the convention by which $\langle H \rangle = v/\sqrt{2}(0, 1)^T$ and $v \simeq 246 \text{ GeV}$.

We notice that other Lorentz and $U(1)_D$ invariant scalars can be constructed with V_μ and derivatives, such as $\partial_\mu V_\rho \partial^\mu \bar{V}^\rho$ or $|\partial_\rho V^\rho|^2$. However they are redundant with $V \bar{V}$ (and current operator, see next) once equations of motion and gauge conditions are imposed, for example $\partial_\mu V_\rho \partial^\mu \bar{V}^\rho = V_\rho \square \bar{V}^\rho + \text{total derivative}$. In addition, there is also the dimension-4 structure $\partial_\mu V^\nu \partial_\nu \bar{V}^\mu$, which after double integration by part can be written as a (symmetric) tensor structure, also to be discussed next.

Vector singlet operators

Lorentz vector operators are again of two types, depending on the CP quantum numbers. In particular we can define a current real CP-even operator and a CP-odd vector exploiting the Levi-Civita tensor

$$\text{vector : } J_\mu^V = i \bar{V}_\nu \overleftrightarrow{\partial}_\mu V^\nu; \quad \text{pseudo - vector : } J_\mu^P = i \epsilon_{\mu\nu\rho\sigma} \bar{V}_\nu \overleftrightarrow{\partial}_\rho V^\sigma. \quad (5)$$

Notice that other CP-even structures such as $\bar{V}^\rho V_{\rho\mu}$ are equivalent to J_μ^V when integration by part and the condition $\partial_\mu V^\mu = 0$ are taken into account. These operators have energy dimension three and can be contracted with vector singlet operators of the SM, such as the hyper-charge current or generic vector structures bilinear in the SM fermions, Higgs and gauge fields. These operators can then be paired with the following vector structures of SM fields:

$$\mathcal{O}_{\text{SM}}^\mu = \{ J_Y^\mu \equiv \frac{\partial^\rho B^\mu{}_\rho}{g'}, J_H^\mu \equiv i H^\dagger \overleftrightarrow{D}^\mu H, \bar{\psi}_i \gamma^\mu \psi_i, \dots \}, \quad (6)$$

where ψ_i denotes a generic SM fermion with flavor index i . For later convenience we have introduced the hyper-charge current J_Y^μ and the Higgs singlet current J_H^μ . We take the complex dark photon to have diagonal couplings to SM fermions, avoiding flavor-violation effects, from which follow equal flavor indices in the fermionic current.

Tensor singlet operators

In principle we can also classify tensor structures and distinguish them upon symmetry properties. In particular we can have both antisymmetric and symmetric combinations:

$$\text{antisymm. : } \mathcal{O}_{\mu\nu}^A = V_{[\mu}\bar{V}_{\nu]}, \quad \mathcal{O}_{\mu\nu}^T = \bar{V}_{[\mu\rho}V_{\nu]}^\rho; \quad \text{symm. : } \mathcal{O}_{\mu\nu}^S = V_{(\mu}\bar{V}_{\nu)}. \quad (7)$$

All these dark operators can be contracted with SM Lorentz tensor structures (also respecting gauge invariance), but notice that if contracted with terms proportional to $g_{\mu\nu}$ the resulting interactions are either redundant with the ones associated to scalar-scalar contact operators or vanish. The $\mathcal{O}_{\mu\nu}^A$ and $\mathcal{O}_{\mu\nu}^S$ terms are dimension 2, but only the antisymmetric combination allows for the creation of a dimension-4 renormalizable interaction when coupled to $B_{\mu\nu}$, therefore resulting of particular interest since it provides leading phenomenological contributions. Meanwhile $\mathcal{O}_{\mu\nu}^T$, that is the traceless part of the complex dark photon stress tensor, and $\mathcal{O}_{\mu\nu}^S$ when contracted with tensor structure with SM fields gives rise to higher dimensional effective operators. We remind that we do not consider operators in $\mathcal{L}_{\text{eff}}(\text{SM}; V_\mu)$ bigger than dimension-6.

Having this in mind, dark tensor singlets can be coupled to the following SM tensor and gauge singlets:

$$\mathcal{O}_{\text{SM}}^{\mu\nu} = \{ B^{\mu\nu}, |H|^2 B^{\mu\nu}, \tilde{B}^{\mu\nu}, |H|^2 \tilde{B}^{\mu\nu}, \partial^{(\mu}\partial^{\nu)}|H|^2, T_\psi^{\mu\nu}, T_F^{\mu\nu} \}. \quad (8)$$

We here accounted for the possibility of giving rise to both CP-even and CP-odd interactions, where the couplings to the hodge dual $\tilde{B}^{\mu\nu}$ is the only extra source of CP-violation coming with SM structures. The tensor structure $T_{\psi(F)}^{\mu\nu}$ is nothing but the energy-momentum tensor of SM fermions (gauge bosons).

We summarize all the possible UV operator structures respecting symmetry constraints with two complex dark photons in table 1.

2.2 Stueckelberg effective field theory

An important consideration on the validity of the EFT is somehow already hidden in eq.(1) when a bare mass term for the vector has been introduced, with the same structure of the operator \mathcal{O}_S .

The free part of eq. (1) enjoys the typical structure of Stueckelberg massive vector, which in isolation is a renormalizable theory. However, interactions can easily spoil this behaviour, as we now show. This is crucially related to the operator \mathcal{O}_S which is badly behaved at high-energy when tested in connection with other interactions and it is of great importance for our effective description. Similar discussions along this line can be found in [44] for a real massive Stueckelberg vector, and in [61] for the case of complex vector only coupled to operators made with electromagnetic field strength. We generalize the discussion to an EFT approach.

In order to illustrate the problem, let us consider as an example the operator $\kappa|H|^2\mathcal{O}_S$, which has exactly the same structure of the mass term, $M^2\mathcal{O}_S$, of eq. (1). Having added interactions, despite them being dimension-4 at this level, and hence *naively* renormalizable, they completely spoil the argument that the Stueckelberg mass can be extrapolated up to extremely high energy. This follows from the

fact that the amplitude for the scattering $hh \rightarrow V\bar{V}$ grows with energy for $E \gg M/\sqrt{\kappa}$, introducing a physical cut-off at a scale $\Lambda \approx M/\sqrt{\kappa}$.

The apparent renormalizability of $\kappa|H|^2V_\mu\bar{V}^\mu$ is manifestly lost when, applying the ‘Stueckelberg trick,’ we restore the gauge invariance of the free Proca Lagrangian. Introducing the Goldstone π and by sending $V_\mu \rightarrow V_\mu + \partial_\mu\pi/M$, we restore the full gauge symmetry under which π shifts. In particular the gauge invariance is realised as

$$\delta V_\mu(x) = \partial_\mu\lambda(x), \quad \delta\pi(x) = -M\lambda(x), \quad (9)$$

and complex conjugate transformations for \bar{V} and $\bar{\pi}$.

This is instrumental to study the high energy behaviour of the model: when discussing the $E \gg M$ limit it is convenient to restore the gauge symmetry. This leads to the following Lagrangian from the free part of (1)

$$\mathcal{L}_V^{\text{Stueckelberg}} = -\frac{1}{2}V_{\mu\nu}\bar{V}^{\mu\nu} + M^2\left(V_\mu + \frac{\partial_\mu\pi}{M}\right)\left(\bar{V}^\mu + \frac{\partial^\mu\bar{\pi}}{M}\right) - \frac{1}{\xi}(\partial_\mu\bar{V}^\mu + \xi M\bar{\pi})(\partial_\mu V^\mu + \xi M\pi), \quad (10)$$

where we have added a R_ξ gauge fixing to remove the $V - \pi$ mixing. In Landau gauge with $\xi = 0$, the amplitudes with an external longitudinal polarization at high momentum $p \gg M$ are equivalent to $\mathcal{A}(V_L(p); \dots) = \epsilon_L^\mu(p)\mathcal{A}_\mu = \mathcal{A}(\pi; \dots)$ as dictated by the ‘equivalence theorem’.

This can then be used to study the high energy behaviour of operators constructed with V_μ . This feature does not appear in operators involving $V_{\mu\nu}$, since it is invariant under (9) and the Goldstone boson π does not appear. Each time an insertion of V_μ is present, the high energy behavior can be studied focusing on the longitudinal polarization of V (in Landau gauge for simplicity). This has remarkable consequences for our DM EFT, for all kind of dark operator structures.

This can then be applied to study the cut-off associated to processes involving non gauge-invariant operators under the sole $\delta V_\mu = \partial_\mu\lambda$. Only operators constructed with $V_{\mu\nu}$ are gauge invariant, while \mathcal{O}_S , J_μ^V , $\mathcal{O}_{\mu\nu}^A$ and $\mathcal{O}_{\mu\nu}^S$ are not. This implies that operators involving such terms are originating from integrating out (at tree or loop level) dark sector states that are involved with the generation of the mass scale M . It also makes evident that only in the singular limit where the Wilson coefficients of these operators are exactly zero the gauge invariance is recovered in the effective operators. In such a limit a local $U(1)^2 \times \mathbb{Z}_2$ is recovered.

For all processes at energies much above M , such as the case of H and Z decays into dark matter, the behavior of this operator is respectively

$$\mathcal{O}_S = \frac{1}{M^2}|\partial_\mu\pi|^2 + \dots, \quad J_\mu^V = \frac{i}{M^2}(\partial_\rho\bar{\pi}\overleftrightarrow{\partial}_\mu^\rho\partial^\rho\pi) + \dots, \quad \mathcal{O}_{\mu\nu} = \frac{\partial_\mu\pi\partial_\nu\bar{\pi}}{M^2} + \dots \quad (11)$$

This signals the appearance of a physical cut-off that can be parametrically smaller than M_\star and it is related to the mass M rather than to some UV parameter.

For the case of interest $|H|^2\mathcal{O}_S$, which will be extremely relevant for our phenomenological discussion, we then have

$$\kappa|H|^2\mathcal{O}_S = \frac{\kappa}{M^2}|H|^2(\partial_\mu\pi + \dots)(\partial^\mu\bar{\pi} + \dots). \quad (12)$$

The operator has a hidden cut-off which is much smaller than naively expected and, as mentioned above, is of order $M/\sqrt{\kappa}$. At this point, our normalization of the $\widehat{\mathcal{L}}_{\text{eff}}$ term in (2) is justified even for the operator $|H|^2\mathcal{O}_S$ and it suggests that the correct power counting for κ is of the form $\kappa \propto \lambda \times (M/M_\star)^2$. Here λ is a (quartic) coupling and M_\star the scale of the new-physics generating the effective interaction. The physical cut-off of the effective operator is now $M_\star/\sqrt{\lambda}$, which is correctly the scale of new-physics M_\star times the effect of the coupling between the SM and DM sectors.

3 Structure of the EFT

Having discussed the possible operators constructed with V_μ invariant under $U(1)_D$ and the constraints on the size of the coupling due to the parametrization as a Stueckelberg massive vector, we are now in the position to write down the effective lagrangian of SM plus DM. As already mentioned, this lagrangian has to be invariant under $SM \times U(1)_D$. At energies below M_\star the SM is deformed by the following interactions

$$\mathcal{L} = \mathcal{L}_{SM} - \frac{1}{2} V_{\mu\nu} \bar{V}^{\mu\nu} + M^2 V_\mu \bar{V}^\mu + \widehat{\mathcal{L}}_{\text{eff}}(\text{SM}; V_\mu) + \frac{1}{M_\star^2} \widehat{\mathcal{L}}_{SM,6}. \quad (13)$$

We have included also the SM EFT at dimension-6, $\widehat{\mathcal{L}}_{SM,6}$, because in concrete realizations we expect that deformations with only SM field be generated by integrating out the dark sector at the scale M_\star . For the moment, we only consider $\widehat{\mathcal{L}}_{\text{eff}}$. The construction of the EFT can proceed simply by listing all the operators of a given dimension built from SM singlet operators and DM singlet operators, in order to have an EFT invariant under $U(1)_D$. Therefore we have

$$\widehat{\mathcal{L}}_{\text{eff}}(\text{SM}; V_\mu) = \widehat{\mathcal{L}}_{\text{eff}}^{(4)} + \frac{1}{M_\star^2} \widehat{\mathcal{L}}_{\text{eff}}^{(6)} + \dots \quad (14)$$

The structure of these two terms is provided below and it is constructed using the operators in table 1 together with the SM structures listed in eqs. (4), (6) and (8).

Dimension-4 terms

There are only three operators at dimension-4, given by

$$\widehat{\mathcal{L}}_{\text{eff}}^{(4)} = \lambda_H \mathcal{O}_S |H|^2 + \lambda_B \mathcal{O}_{\mu\nu}^A B^{\mu\nu} + \lambda'_B \mathcal{O}_{\mu\nu}^A \tilde{B}^{\mu\nu}. \quad (15)$$

While the first term is common to any theory of dark photon, and it is essentially an Higgs-portal interaction, the second and third contributions only arise for complex dark photon scenarios, since the anti-symmetric two index tensor vanishes for real vectors. In particular, we are interested in the phenomenology associated to the λ_B , λ'_B coefficients, which induce a low-energy interaction between DM and the photon – despite the complex dark photon being electrically neutral. These interactions can give enhanced features at low momentum transferred in direct detection, equivalent to magnetic and electric dipole moment for spin-1 dark matter respectively [45, 61, 62]. Being dimension four, the operators in eq. (15) are expected to be the leading effect, which should be even more important for strongly coupled DM as in [63]. However, we will see that the appropriate power counting connected to the discussion in sec. 2.2 will make the size of the Wilson coefficients effectively smaller.

name	expression	naive	improved power-counting
\mathcal{O}_S	$V_\mu \bar{V}^\mu$	1	$\times (M/M_\star)^2$
\mathcal{O}_{F^2}	$V_{\mu\nu} \bar{V}^{\mu\nu}$	1	1
\mathcal{O}_P	$\epsilon_{\mu\nu\rho\sigma} V^{\mu\nu} \bar{V}^{\rho\sigma}$	1	1
J_μ^V	$i \bar{V}_\nu \overleftrightarrow{\partial}_\mu V^\nu$	1	$\times (M/M_\star)^2$
J_μ^P	$i \epsilon^{\mu\nu\rho\sigma} \bar{V}_\nu \overleftrightarrow{\partial}_\rho V_\sigma$	1	$\times (M/M_\star)^2$
$\mathcal{O}_{\mu\nu}^S$	$V_{(\mu} \bar{V}_{\nu)}$	1	$\times (M/M_\star)^2$
$\mathcal{O}_{\mu\nu}^A$	$V_{[\mu} \bar{V}_{\nu]}$	1	$\times (M/M_\star)^2$
$\mathcal{O}_{\mu\nu}^T$	$V_{[\mu\rho} \bar{V}^{\rho}_{\nu]}$	1	1

Table 2. We summarize the effect of the application of the *improved power counting* of eq.(17) to all of the possible DM structures listed in tab.1, highlighting when the extra (M^2/M_\star^2) factor modifies the usual *naive power counting*.

Dimension-6 terms

There are clearly many more operators at dimension 6; they are given by the following Lagrangian:

$$\begin{aligned}
\widehat{\mathcal{L}}_{\text{eff}}^{(6)} = & \mathcal{O}_S \left[\mathcal{C}_H |H|^4 + \mathcal{C}_{DH} |D_\mu H|^2 + \sum_\psi \mathcal{C}_{H\psi} y_\psi \bar{\psi} H \psi + \sum_F \left(\mathcal{C}_F F_{\mu\nu} F^{\mu\nu} + \mathcal{C}_{\tilde{F}} F_{\mu\nu} \tilde{F}^{\mu\nu} \right) \right] \\
& + \mathcal{C}_{H,2} \mathcal{O}_{F^2} |H|^2 + \mathcal{C}_{H,3} \mathcal{O}_P |H|^2 \\
& + J_\mu^V \left[\sum_\psi \mathcal{C}_\psi \bar{\psi} \gamma^\mu \psi + \mathcal{C}_Y J_Y^\mu + \mathcal{C}_{Hc} J_H^\mu \right] + J_\mu^P \left[\sum_\psi \mathcal{C}_{\tilde{\psi}} \bar{\psi} \gamma^\mu \psi + \mathcal{C}_{\tilde{Y}} J_Y^\mu + \mathcal{C}_{\tilde{H}c} J_H^\mu \right] \\
& + \mathcal{O}_{\mu\nu}^S \left[\mathcal{C}_{D^2H} \partial^{(\mu} \partial^{\nu)} |H|^2 + \sum_\psi \mathcal{C}_{T_\psi} T_\psi^{\mu\nu} + \sum_q \mathcal{C}_{T_F} T_F^{\mu\nu} \right] \\
& + \mathcal{O}_{\mu\nu}^A \left[\mathcal{C}_{HB} |H|^2 B^{\mu\nu} + \sum_\psi \mathcal{C}_{H\psi,2} y_\psi \bar{\psi} H \sigma^{\mu\nu} \psi \right] + \mathcal{C}_B \mathcal{O}_{\mu\nu}^T B^{\mu\nu} \\
& + \mathcal{O}_{\mu\nu}^A \mathcal{C}'_{HB} |H|^2 \tilde{B}^{\mu\nu} + \epsilon^{\mu\nu\rho\sigma} \mathcal{O}_{\mu\nu}^A \sum_\psi \mathcal{C}_{H\psi,3} y_\psi \bar{\psi} H \sigma_{\rho\sigma} \psi + \mathcal{C}'_B \mathcal{O}_{\mu\nu}^T \tilde{B}^{\mu\nu} .
\end{aligned} \tag{16}$$

We have grouped the various contact interaction accordingly to their Lorentz structure. We explicitly multiply every interaction involving one left handed and one right handed SM fermion by the corresponding Yukawa coupling, in such a way that Minimal Flavor Violation is respected [64].

3.1 Power counting possibilities

We would now like to assign to the various coefficients a natural size that respects a good high-energy behavior of the theory, consistent with having massive gauge fields in the EFT. Exploiting the discussion of section 2.2, we can argue in favor of the following power counting: every vector field V_μ that appears without the full field strength is assigned a weight

$$V_\mu \rightarrow \frac{M}{M_\star} V_\mu \quad \text{improved power-counting} \tag{17}$$

\mathcal{C}_i	Power counting	\mathcal{C}_i	Power counting	\mathcal{C}_i	Power counting
\mathcal{C}_H	$c_H g_\star^4$	\mathcal{C}_{DH}	$c_{DH} g_\star^2$	$\mathcal{C}_{H\psi}$	$c_{H\psi} g_\star^2$
$\mathcal{C}_{F, \tilde{F}}$	$g_F^2 c_{F, \tilde{F}} \frac{g_\star^2}{16\pi^2}$	$\mathcal{C}_{H,2}$	$c_{H,2} g_\star^2 \frac{g_\star^2}{16\pi^2}$	$\mathcal{C}_{H,3}$	$c_{H,3} g_\star^2 \frac{g_\star^2}{16\pi^2}$
$\mathcal{C}_{\psi, Y, Hc}$	$c_{\psi, Y, Hc} g_\star^2$	$\mathcal{C}_{\tilde{\psi}, \tilde{Y}, \tilde{H}c}$	$c_{\tilde{\psi}, \tilde{Y}, \tilde{H}c} g_\star^2$	\mathcal{C}_{D2H}	$c_{D2H} g_\star^2$
\mathcal{C}_{T_ψ}	$c_{T_\psi} g_\star^2$	\mathcal{C}_{T_F}	$c_{T_F} g_\star^2$	\mathcal{C}_{HB}	$c_{HB} g_Y g_\star^2 \frac{g_\star^2}{16\pi^2}$
$\mathcal{C}_{H\psi,2}$	$c_{H\psi,2} g_\star^2$	\mathcal{C}_B	$c_B g_Y \frac{g_\star^2}{16\pi^2}$	\mathcal{C}'_{HB}	$c'_{HB} g_Y g_\star^2 \frac{g_\star^2}{16\pi^2}$
$\mathcal{C}_{H\psi,3}$	$c_{H\psi,3} g_\star^2$	\mathcal{C}'_B	$c'_B g_Y \frac{g_\star^2}{16\pi^2}$		

Table 3. List of the normalized effective Wilson coefficients for dimension 6 operators in terms of powers of gauge couplings g_i .

In principle this rescaling has an overall $O(1)$ dimensionless coefficient that we fix to unity in the rest of the paper (see however section 6).

The rescaling of eq. (17) has several effects. First of all, while it does not change the dimensionality of the operators, it makes their Wilson coefficient consistent with a high-energy limit of the massive gauge field, as discussed in section 2.2. Second, it will guarantee a correct high-energy behaviour, namely when the energy is in the range $M \ll E \ll M_\star$, we will not see spurious non-decoupling effects, which is instrumental for a correct interpretation of the collider bounds. This has also an impact for the low energy physics related to DM scatterings (and, in general, also annihilations), since it naturally suppresses the size of the effects by the DM mass. Therefore, although less spectacular than the effects on high-energy observables $M \ll E$, there are important consequences also at low energies.

In terms of operators, this implies that the Wilson coefficients should be rescaled according to what shown in table 2. In the table, we contrast the improved power-counting introduced in eq. (17) with the naive power-counting in which the V_μ rescaling is not applied.

Moreover, in order to make a stronger connection with possible UV completion, we define the size of the Wilson coefficient \mathcal{C}_i normalized (in \hbar counting) to a coupling g_\star . Every coefficient \mathcal{C}_i in eq. (14) therefore has its explicit expression in terms of g_\star . The dictionary is the following: for dimension 4 operators, we have

$$\left\{ \lambda_H = d_H g_\star^2, \quad \lambda_B = d_B g_Y \frac{g_\star^2}{16\pi^2}, \quad \lambda'_B = d'_B g_Y \frac{g_\star^2}{16\pi^2} \right\}, \quad (18)$$

where g_Y is the hyper-charge gauge coupling and all the small d 's are $O(1)$ numbers. The same can be done at the level of dimension 6 operators, for which we obtain the expressions summarized in table 3, where g_F denotes the gauge coupling of the gauge boson $F = G, W, B$ and the c 's are $O(1)$ numbers.

3.2 About the dark photon physical mass

The first terms of (15) and (16) renormalize the low-energy free lagrangian of V_μ . Indeed, upon electroweak symmetry breaking they redefine the dark photon mass as

$$M_{\text{phys}}^2 = M^2 \left[1 + d_H \frac{g_\star^2 v^2}{M_\star^2} + \frac{c_H}{2} \left(\frac{g_\star^2 v^2}{M_\star^2} \right)^2 \right]. \quad (19)$$

With the improved power counting, the physical mass is only partially corrected by higher dimensional operators, since if $M \rightarrow 0$ in the above formula the physical mass is itself zero. Also the correction from c_H is quadratically suppressed as compared to λ_H .

There are, however, two more extreme Stueckelberg-like scenarios. First, the case $M \gg g_* v$, where the physical mass originates mostly from dynamics above M_* in such a way that M corrections to the mass can be neglected. In this limit one could explore a Stueckelberg-like interactions with $|H|^{2n}$ without the suppression M^{2n}/M_*^{2n} . In particular we reach this configuration with the shift $\lambda_H \rightarrow \lambda_H^S \times M_*^2/M^2$. The cut-off scale of our EFT becomes $E \gtrsim M/\sqrt{\lambda_H} g_*$. Second, we have the pure massless Stueckelberg scenario, where V gets its mass entirely from $|H|^2$. This limit can be reached by rescaling $\lambda_H \rightarrow \lambda_H^0 \times M_*^2/M^2$ and $\mathcal{C}_{H,2} \rightarrow \mathcal{C}_{H,2}^0 \times M_*^4/M^4$ and then also $M \rightarrow 0$. Such a term has an even lower cut-off than the one discussed in section 2.2, since in the limit where $M \rightarrow 0$ the physical mass does not vanish, but its proportional to $M_{\text{phys}} \propto \lambda_H^0 g_* v$. Such a limit shows a cut-off in the scattering $hh \rightarrow V\bar{V}$ at around $E \gtrsim v$, which is as worse as the one of Higgsless theories. We will briefly come back to this case in section 5.2 where we explore whether this scenario can live in some point of the parameters space tested by experiments. Notice that, upon electro-weak symmetry breaking, the first operator on the second line of (16) renormalizes the wave-function of V_μ . We neglect this correction, since in minimally coupled models it arises at loop-level.

4 Matching onto low energy EFT

The EFT so far developed in eq. (14) cannot be used straightforwardly unless we are just interested in high energy phenomena, as, for example, modifications to invisible branching ratios of H and Z (as discussed in section 5.1). When we are interested in low energy phenomena like direct detection experiments, we would like to match our eq. (14) to a non-relativistic theory of nuclei.

In this section we discuss in detail the procedure to match our EFT onto effective theories valid at even lower energy regimes. While this procedure is completely standard (see [65] for a technical review), this exercise will allow us to keep track explicitly of all the operators in eq. (14) by computing their effects on low-energy observables. A summary of the low energy operators generated in our model is shown in two main tables: table 4 for the EFT of DM and quarks and gluons; table 5 for the non-relativistic EFT of DM-nucleons.

4.1 Matching at the Electro-Weak Scale

According to our fundamental assumptions, our EFT is defined at the UV scale $M_* \gg M_{\text{EW}}$ at which any heavy dark degree of freedom is integrated out. Moving to lower energies, we need to perform a first matching procedure at the electroweak scale, when the Z , W , h bosons and the heavy top-quark must be integrated out. The effective Lagrangian valid at energies $E \ll M_{\text{EW}}$ is generally given by:

$$\mathcal{L}_{\text{EFT}}|_{E \ll M_{\text{EW}}} \supset \sum_{i=1}^{22} \tilde{c}_i \tilde{\mathcal{O}}_i, \quad (20)$$

with the operators $\tilde{\mathcal{O}}_i$ and the corresponding Wilson coefficients \tilde{c}_i listed in table 4. In the table, we write the SM structures to be further evaluated when even lower energies are considered (see next section) in square brackets, and we also show in square brackets the two possible power counting choices according to what stated in table 2.

$\tilde{\mathcal{O}}_i$	\tilde{c}_i
$\tilde{\mathcal{O}}_1 = V_\mu \bar{V}^\mu [m_q \bar{q} q]$	$\tilde{c}_1 = [1, \frac{M^2}{M_*^2}] (-\frac{\lambda_H}{M_h^2} - \frac{C_H}{M_*^2} \frac{v^2}{M_h^2} + \frac{C_{Hf}}{M_*^2})$
$\tilde{\mathcal{O}}_2 = V_\mu \bar{V}^\mu [\frac{\alpha_s}{12\pi} G_{\mu\nu} G^{\mu\nu}]$	$\tilde{c}_2 = [1, \frac{M^2}{M_*^2}] (\frac{\lambda_H}{M_h^2} + \frac{C_H}{M_*^2} \frac{v^2}{M_h^2} + \frac{C_F}{M_*^2})$
$\tilde{\mathcal{O}}_3 = V_{\mu\nu} \bar{V}^{\mu\nu} [m_q \bar{q} q]$	$\tilde{c}_3 = -\frac{C_{H,2}}{M_*^2 M_h^2}$
$\tilde{\mathcal{O}}_4 = V_{\mu\nu} \bar{V}^{\mu\nu} [\frac{\alpha_s}{12\pi} G_{\mu\nu} G^{\mu\nu}]$	$\tilde{c}_4 = -\frac{C_{H,2}}{M_*^2 M_h^2}$
$\tilde{\mathcal{O}}_5 = \tilde{V}_{\mu\nu} \bar{V}^{\mu\nu} [m_q \bar{q} q]$	$\tilde{c}_5 = -\frac{C_{H,3}}{M_*^2 M_h^2}$
$\tilde{\mathcal{O}}_6 = \tilde{V}_{\mu\nu} \bar{V}^{\mu\nu} [\frac{\alpha_s}{12\pi} G_{\mu\nu} G^{\mu\nu}]$	$\tilde{c}_6 = -\frac{C_{H,3}}{M_*^2 M_h^2}$
$\tilde{\mathcal{O}}_7 = J_\mu^V [J_q^\mu]$	$\tilde{c}_7 = [1, \frac{M^2}{M_*^2}] \frac{1}{M_*^2} (C_f + C_Y Y_f + C_{Hc} \frac{g_Z^2 g_v^q v^2}{M_Z^2})$
$\tilde{\mathcal{O}}_8 = J_\mu^P [J_q^\mu]$	$\tilde{c}_8 = [1, \frac{M^2}{M_*^2}] \frac{g_Z^2}{M_*^2} (C_{\tilde{f}} + C_{\tilde{Y}} Y_f + C_{\tilde{H}c} \frac{g_Z^2 g_v^q v^2}{M_Z^2})$
$\tilde{\mathcal{O}}_9 = V_{[\mu} \bar{V}_{\nu]} [F^{\mu\nu}]$	$\tilde{c}_9 = [1, \frac{M^2}{M_*^2}] \frac{c_{\theta_w}}{2} (\lambda_B + C_{HB} \frac{v^2}{M_*^2})$
$\tilde{\mathcal{O}}_{10} = V_{[\mu} \bar{V}_{\nu]} [\bar{q} \sigma^{\mu\nu} q]$	$\tilde{c}_{10} = [1, \frac{M^2}{M_*^2}] \frac{C_{Hf,2}}{2M_*^2} m_q$
$\tilde{\mathcal{O}}_{11} = V_{[\mu} \bar{V}_{\nu]} [\partial^{[\mu} J_{\text{NC}}^{\nu]}]$	$\tilde{c}_{11} = [1, \frac{M^2}{M_*^2}] \frac{s_{\theta_w}}{2} \frac{g_Z}{M_Z^2} (\lambda_B + C_{HB} \frac{v^2}{M_*^2})$
$\tilde{\mathcal{O}}_{12} = V_{[\mu\rho} \bar{V}_{\nu]}^\rho [F^{\mu\nu}]$	$\tilde{c}_{12} = c_{\theta_w} \frac{C_B}{M_*^2}$
$\tilde{\mathcal{O}}_{13} = V_{[\mu\rho} \bar{V}_{\nu]}^\rho [\partial^{[\mu} J_{\text{NC}}^{\nu]}]$	$\tilde{c}_{13} = s_{\theta_w} \frac{g_Z}{M_Z^2} \frac{C_B}{M_*^2}$
$\tilde{\mathcal{O}}_{14} = V_{(\mu} \bar{V}_{\nu)} [T_G^{\mu\nu}]$	$\tilde{c}_{14} = [1, \frac{M^2}{M_*^2}] \frac{C_{TF}}{2M_*^2}$
$\tilde{\mathcal{O}}_{15} = V_{(\mu} \bar{V}_{\nu)} [\partial^{(\mu} J_q^{\nu)}]$	$\tilde{c}_{15} = [1, \frac{M^2}{M_*^2}] \frac{C_{Tf}}{2M_*^2}$
$\tilde{\mathcal{O}}_{16} = V_{(\mu} \bar{V}_{\nu)} [\partial^{(\mu} \partial^{\nu)} m_q \bar{q} q]$	$\tilde{c}_{16} = -[1, \frac{M^2}{M_*^2}] \frac{C_{D2H}}{2M_*^2 M_h^2}$
$\tilde{\mathcal{O}}_{17} = V_{(\mu} \bar{V}_{\nu)} [\partial^{(\mu} \partial^{\nu)} \frac{\alpha_s}{12\pi} G_{\alpha\beta} G^{\alpha\beta}]$	$\tilde{c}_{17} = -[1, \frac{M^2}{M_*^2}] \frac{C_{D2H}}{2M_*^2 M_h^2}$
$\tilde{\mathcal{O}}_{18} = V_{[\mu} \bar{V}_{\nu]} \tilde{F}^{\mu\nu}$	$\tilde{c}_{18} = [1, \frac{M^2}{M_*^2}] \frac{c_{\theta_w}}{2} (\lambda'_B + C'_{HB} \frac{v^2}{M_*^2})$
$\tilde{\mathcal{O}}_{19} = \varepsilon^{\mu\nu\rho\sigma} V_{[\mu} \bar{V}_{\nu]} [\bar{q} \sigma_{\rho\sigma} q]$	$\tilde{c}_{19} = -[1, \frac{M^2}{M_*^2}] \frac{C_{H\psi,3}}{2M_*^2} m_q$
$\tilde{\mathcal{O}}_{20} = \varepsilon^{\mu\nu\rho\sigma} V_{[\mu} \bar{V}_{\nu]} [\partial_{[\mu} J_{\text{NC}} \sigma]]$	$\tilde{c}_{20} = [1, \frac{M^2}{M_*^2}] \frac{s_{\theta_w}}{2} \frac{g_Z}{M_Z^2} (\lambda'_B + C'_{HB} \frac{v^2}{M_*^2})$
$\tilde{\mathcal{O}}_{21} = V_{[\mu\rho} \bar{V}_{\nu]}^\rho [\tilde{F}^{\mu\nu}]$	$\tilde{c}_{21} = c_{\theta_w} \frac{C'_B}{M_*^2}$
$\tilde{\mathcal{O}}_{22} = \varepsilon^{\mu\nu\rho\sigma} V_{[\mu\alpha} \bar{V}_{\nu]}^\alpha [\partial_{[\rho} J_{\text{NC}} \sigma]]$	$\tilde{c}_{22} = s_{\theta_w} \frac{g_Z}{M_Z^2} \frac{C'_B}{M_*^2}$

Table 4. Effective operators involving quarks and gluons, and corresponding Wilson coefficients, obtained matching the EFT presented in section 3 to the low energy EFT of eq. (20) at the weak scale. We set the Wilson coefficients $C_{DH}, C_{D\psi}, C_{\tilde{F}} = 0$ since they will not play any role in the rest of the work. In the second column we indicate in square brackets the two alternative choices for the power counting, i.e. 1 for the *naive* power counting and M^2/M_*^2 for the *improved* power counting.

In order to set the notation, θ_w is the weak angle, the quark current J_q^μ that appears in $\tilde{\mathcal{O}}_{7,8,11,13,15}$ is the vector current $J_q^\mu = \bar{q} \gamma^\mu q$ computed with light quarks, while J_{NC}^μ is the neutral current to which

the Z boson couples,

$$J_{\text{NC}}^\mu = \left(\frac{1}{2} - \frac{4}{3}s_{\theta_w} \right) \bar{u}\gamma^\mu u + \left(-\frac{1}{2} + \frac{2}{3}s_{\theta_w} \right) (\bar{d}\gamma^\mu d + \bar{s}\gamma^\mu s). \quad (21)$$

It appears in the $\tilde{\mathcal{O}}_{11,13,20,22}$ operators because they are obtained integrating out the Z boson in the s-channel (as well as in the contribution from the Higgs current in $\tilde{\mathcal{O}}_{7,8}$ but with a different structure, so we dropped the notation momentarily there). It is trivial to notice that from each coupling of the complex dark photon to the hypercharge, we obtain two contributions below the EW symmetry breaking, among which the one due to the Z -coupling is evidently suppressed by an extra $1/M_Z^2$ factor. On the other hand, the operators $\tilde{\mathcal{O}}_{9,12,18,21}$ that contain a single photon field strength will be particularly important for direct detection, since they contribute to the cross section via a photon exchange in the t-channel and are thus *enhanced*, rather than suppressed, by the small momentum exchanged in the reaction. On top of that, we will only show bounds coming from the γ -coupling when discussing direct detection phenomenology in section 5.2. Finally, $T_G^{\mu\nu}$ denotes the energy-momentum tensor of gluons. We do not consider operators that contain leptons and more than one photon because they are not relevant (at leading order) for the phenomenology we discuss in this work.

4.2 Single Nucleon EFT

We now take the EFT defined by eq. (20) and move to even lower energies. The next relevant threshold we encounter is around the GeV, i.e. around the QCD confinement scale, when we must match to a single-nucleon relativistic EFT. In momentum space, the Lagrangian can be written in terms of the nucleon field N as

$$\begin{aligned} \mathcal{L}_N = & c_S V_\mu \bar{V}^\mu \bar{N} N + c_{FS} V_{\mu\nu} \bar{V}^{\mu\nu} \bar{N} N + c_{PS} \tilde{V}_{\mu\nu} \bar{V}^{\mu\nu} \bar{N} N + c_V J_\mu^V J_N^\mu + c_{PV} J_\mu^P J_N^\mu + c_M V_{[\mu} \bar{V}_{\nu]} q^{[\mu} J_N^{\nu]} \\ & + c_{AT} V_{[\mu} \bar{V}_{\nu]} \bar{N} \sigma^{\mu\nu} N + c'_M V_{[\mu\rho} \bar{V}_{\nu]}^\rho q^{[\mu} J_N^{\nu]} + c_{ST} V_{(\mu} \bar{V}_{\nu)} q^{(\mu} J_N^{\nu)} + c_{2d} V_{(\mu} \bar{V}_{\nu)} q^{(\mu} q^{\nu)} \bar{N} N \\ & + c_E \varepsilon^{\mu\nu\rho\sigma} V_{[\mu} \bar{V}_{\nu]} q_{[\rho} J_{N\sigma]} + c'_{AT} \varepsilon^{\mu\nu\rho\sigma} V_{[\mu} \bar{V}_{\nu]} \bar{N} \sigma_{\rho\sigma} N + c'_E \varepsilon^{\mu\nu\rho\sigma} V_{[\mu\alpha} \bar{V}_{\nu]}^\alpha q_{[\rho} J_{N\sigma]} \end{aligned} \quad (22)$$

where q represents the exchanged 4-momentum and the vector nucleon current is $J_N^\mu = \bar{N}\gamma^\mu N$. The set of effective operators appearing in eq. (22) is obtained by evaluating the operator structures in square brackets containing quarks and gluons that appear in table 4 using the matrix elements listed in [65, 66]. The dimensionful Wilson coefficients appearing in eq. (22) can then be written in terms of

the tilded Wilson coefficients of table 4 as

$$\begin{aligned}
c_S &= m_N \left[\left(\sum_q f_{Tq}^N \right) \tilde{c}_1 + \frac{2}{27} \left(\sum_q f_{Tq}^N - 1 \right) \tilde{c}_2 \right], & c_V &= \sum_q F_1^{q,N}(0) \tilde{c}_7, \\
c_{FS} &= m_N \left[\left(\sum_q f_{Tq}^N \right) \tilde{c}_3 + \frac{2}{27} \left(\sum_q f_{Tq}^N - 1 \right) \tilde{c}_4 \right], & c_{PV} &= \sum_q F_1^{q,N}(0) \tilde{c}_8, \\
c_{PS} &= m_N \left[\left(\sum_q f_{Tq}^N \right) \tilde{c}_5 + \frac{2}{27} \left(\sum_q f_{Tq}^N - 1 \right) \tilde{c}_6 \right], & c_{AT} &= \sum_q F_{T,0}^{q,N}(0) \tilde{c}_{10}, \\
c_{2d} &= m_N \left[\left(\sum_q f_{Tq}^N \right) \tilde{c}_{16} + \frac{2}{27} \left(\sum_q f_{Tq}^N - 1 \right) \tilde{c}_{17} \right], & c_{ST} &= \sum_q F_1^{q,N}(0) \tilde{c}_{15}, \\
c_M &= \frac{Q_N}{q^2} \tilde{c}_9 + F_1^{\text{NC}}(0) \tilde{c}_{11}, & c'_M &= \frac{Q_N}{q^2} \tilde{c}_{12} + F_1^{\text{NC}}(0) \tilde{c}_{13}, \\
c_E &= \frac{Q_N}{q^2} \tilde{c}_{18} + F_1^{\text{NC}}(0) \tilde{c}_{20}, & c'_E &= \frac{Q_N}{q^2} \tilde{c}_{21} + F_1^{\text{NC}}(0) \tilde{c}_{22}, \\
c'_{AT} &= \sum_q F_{T,0}^{q,N}(0) \tilde{c}_{19}, & &
\end{aligned} \tag{23}$$

where we used the standard notation for the form factors that appear at the nucleon level (see [65, 66]). The effective coefficients generated by UV interactions to the hypercharge are here labelled according to the type of interaction they resemble, *i.e.* $c_M^{(\prime)}$ contributes to the complex dark photon magnetic dipole while $c^{(\prime)}E$ is the triggered electric dipole-like coupling.

4.3 Non-relativistic Effective Field Theory

Finally, the relativistic EFT defined in eq. (22) should be reduced to a non-relativistic EFT (NREFT), that can be used to compute nuclear response functions needed for the purpose of direct detection. Such a NREFT can be written in terms of the following independent Galilean invariants:

$$\left\{ \mathcal{I}_{V,N}, \vec{q} = \vec{p} - \vec{p}' = \vec{k} - \vec{k}', \vec{P} = \vec{p} + \vec{p}', \vec{v}_\perp = \frac{\vec{P}}{2M} - \frac{\vec{P}_N}{2m_N}, \vec{P}_N = \vec{k} + \vec{k}', \vec{S}_V, \vec{s}_N, \mathcal{S} \right\}, \tag{24}$$

where $\mathcal{I}_{V,N}$ is the identity operator acting in the dark photon (V) or nucleon (N) space, \vec{p} and \vec{p}' are the initial and final DM momenta, \vec{k} and \vec{k}' are the initial and final nuclear momenta, \vec{S}_V and \mathcal{S} are the complex dark photon spin operators (we defer to appendix A for the definition of such operators for spin-1 DM), \vec{s}_N represents the nucleon spin and \vec{v}_\perp is the so called transverse velocity.

The NREFT Lagrangian is constructed out of Galilean and rotational invariant combinations of the structures presented in eq. (24) and explicitly reads

$$\mathcal{L}_{\text{NR}} = \sum_{i=1}^{25} \sum_N c_i^N \mathcal{O}_i^{\text{NR}}, \tag{25}$$

This ‘‘Lagrangian’’ must be interpreted as the matrix element of the direct detection scattering process, as is clear from its dimensions, computed for a set of hermitian operators that were classified in

$\mathcal{O}_i^{\text{NR}}$	Structure	\mathcal{C}_i	$\mathcal{O}_i^{\text{NR}}$	Structure	\mathcal{C}_i
$\mathcal{O}_1^{\text{NR}}$	1	$\lambda_H, \mathcal{C}_{H,2}, \mathcal{C}_F, \mathcal{C}_\psi$	$\mathcal{O}_{13}^{\text{NR}}$	$i(\vec{S}_V \cdot \vec{v}_\perp)(\vec{q} \cdot \vec{s}_N)/m_N$	
$\mathcal{O}_2^{\text{NR}}$	v_\perp^2	not generated	$\mathcal{O}_{14}^{\text{NR}}$	$i(\vec{s}_N \cdot \vec{v}_\perp)(\vec{q} \cdot \vec{S}_V)/m_N$	
$\mathcal{O}_3^{\text{NR}}$	$i\vec{s}_N \cdot (\vec{q} \times \vec{v}_\perp)/m_N$		$\mathcal{O}_{15}^{\text{NR}}$	$(\vec{S}_V \cdot \vec{q})[(\vec{s}_N \times \vec{v}_\perp) \cdot \vec{q}]/m_N^2$	
$\mathcal{O}_4^{\text{NR}}$	$\vec{S}_V \cdot \vec{s}_N$		$\mathcal{O}_{16}^{\text{NR}}$	$[\vec{S}_V \cdot (\vec{q} \times \vec{v}_\perp)](\vec{q} \cdot \vec{s}_N)/m_N^2$	
$\mathcal{O}_5^{\text{NR}}$	$i\vec{S}_V \cdot (\vec{q} \times \vec{v}_\perp)/m_N$	λ_B, \mathcal{C}_B	$\mathcal{O}_{17}^{\text{NR}}$	$iq^i \mathcal{S}_{ij} v_\perp^j / m_N$	$\mathcal{C}_{T\psi}$
$\mathcal{O}_6^{\text{NR}}$	$(\vec{S}_V \cdot \vec{q})(\vec{s}_N \cdot \vec{q})/m_N^2$		$\mathcal{O}_{18}^{\text{NR}}$	$iq^i \mathcal{S}_{ij} s_N^j / m_N$	
$\mathcal{O}_7^{\text{NR}}$	$\vec{s}_N \cdot \vec{v}_\perp$		$\mathcal{O}_{19}^{\text{NR}}$	$q^i q^j \mathcal{S}_{ij} / m_N^2$	$\mathcal{C}_{H\psi,2}, \mathcal{C}_{D2H}$
$\mathcal{O}_8^{\text{NR}}$	$\vec{S}_V \cdot \vec{v}_\perp$	$\mathcal{C}_{\tilde{\psi}}$	$\mathcal{O}_{20}^{\text{NR}}$	$[(\vec{s}_N \times \vec{q})^i q^j \mathcal{S}_{ij} / m_N^2$	
$\mathcal{O}_9^{\text{NR}}$	$i\vec{S}_V \cdot (\vec{s}_N \times \vec{q})/m_N$		$\mathcal{O}_{21}^{\text{NR}}$	$v_\perp^i s_N^j \mathcal{S}_{ij}$	
$\mathcal{O}_{10}^{\text{NR}}$	$i(\vec{q} \cdot \vec{s}_N)/m_N$		$\mathcal{O}_{22}^{\text{NR}}$	$i[(\vec{q} \times \vec{v}_\perp)]^i s_N^j \mathcal{S}_{ij} / m_N$	
$\mathcal{O}_{11}^{\text{NR}}$	$i(\vec{q} \cdot \vec{S}_V)/m_N$	$\mathcal{C}_{H,3}, \lambda'_B, \mathcal{C}'_B, \mathcal{C}_{H\psi,3}$	$\mathcal{O}_{23}^{\text{NR}}$	$i[(\vec{s}_N \times \vec{v}_\perp)]^i q^j \mathcal{S}_{ij} / m_N$	
$\mathcal{O}_{12}^{\text{NR}}$	$\vec{S}_V \cdot (\vec{s}_N \times \vec{v}_\perp)$		$\mathcal{O}_{24}^{\text{NR}}$	$i[(\vec{s}_N \times \vec{q})^i v_\perp^j \mathcal{S}_{ij} / m_N$	
			$\mathcal{O}_{25}^{\text{NR}}$	$v_\perp^i v_\perp^j \mathcal{S}_{ij}$	not generated

Table 5. Basis of non-relativistic operators for direct detection of complex spin-1 DM. The first column shows the usual non redundant basis constructed with a single structure. Operators \mathcal{O}_i exclusive for spin-1 DM starts from $i \geq 17$. Spin-independent operators have been highlighted and we point to the leading contribution from UV Wilson coefficient that generate each specific interaction, with the complete matching given in eq. (26).

[67, 68] and augmented in [69–71] to take into account the additional structures that appear for spin-1 DM. We provide the complete set of invariant structures in table 5. Since our focus in section 5.2 will be exclusively on spin-independent cross-sections, in the table we highlight in green the operators that are relevant for our purpose and we point to the relative leading contribution in terms of the coefficients for the high energy effective theory presented in section 3.

We match the single nucleon EFT of eq. (22) onto eq. (25) and obtain the following results for the Wilson coefficients generating spin-independent interactions:

$$\begin{aligned}
c_1^N &= -2m_N (c_S + 2M^2 c_{FS} + 2M c_V) && \leftarrow \{ \lambda_H, \mathcal{C}_H, \mathcal{C}_{H\psi}, \mathcal{C}_F, \mathcal{C}_{H,2}, \mathcal{C}_{\psi, Y, Hc} \}, \\
c_2^N &= \text{Not generated} && \leftarrow \{ \}, \\
c_5^N &= 4m_N^2 (-c_\mu + M^2 c'_\mu) && \leftarrow \{ \lambda_B, \mathcal{C}_{HB}, \mathcal{C}_B \}, \\
c_8^N &= -4M m_N c_{PV} && \leftarrow \{ \mathcal{C}_{\tilde{\psi}, \tilde{Y} \tilde{H}c} \}, \\
c_{11}^N &= -2m_N (4M m_N c_{PS} + c'_{AT} + 2m_N c_D + 2M^2 m_N c'_D) && \leftarrow \{ \mathcal{C}_{H,3}, \mathcal{C}_{H\psi,3}, \lambda'_B, \mathcal{C}'_{HB}, \mathcal{C}'_B \}, \\
c_{17}^N &= -8m_N^2 c_{ST} && \leftarrow \{ \mathcal{C}_{T\psi} \}, \\
c_{19}^N &= 2m_N^2 \left(4m_N c_{2D} + \frac{c_{AT}}{M} \right) && \leftarrow \{ \mathcal{C}_{D2H}, \mathcal{C}_{H\psi,2} \}, \\
c_{25}^N &= \text{Not generated} && \leftarrow \{ \}.
\end{aligned} \tag{26}$$

For each entry, we also list the high-energy Wilson coefficients that contribute to the low energy coefficients c_i^N . We observe that c_5^N is enhanced by a factor $1/\bar{q}^2$ contained in $c_M^{(\prime)}$ and the same applies to the $c_E^{(\prime)}$ contribution to the NR Lagrangian coefficient c_{11}^N . This factor comes from the photon exchange and is generated by the magnetic ($\tilde{\mathcal{O}}_9, \tilde{\mathcal{O}}_{12}$) and electric ($\tilde{\mathcal{O}}_{18}, \tilde{\mathcal{O}}_{21}$) “dipole-like” interactions

appearing in table 4, respectively. We stress that we keep only the leading contributions generated by each of the operators in eq. (22) in a q^n expansion, neglecting for instance higher order terms like $c_5 \mathcal{O}_{19}^{\text{NR}} \sim O(q^2)$ or $c_M q^2 \mathcal{O}_1^{\text{NR}}$ which does not show the $1/q^2$ enhancement for dipole-like interactions we just mentioned.

5 Phenomenological Bounds

The main focus of this section are phenomenological constraints on our EFT. In this section we derive bounds on the Wilson coefficients with particular emphasis on the improved power counting. For this very same reason, prior to the discussion of direct detection, we also consider collider bounds coming from invisible decays of the Higgs and Z bosons. This will serve us as a proof of the importance of this approach in deriving sensible limits, as we will show how an incorrect treatment of the cut-off of massive Stueckelberg would lead to spurious very strong bounds.

In this section, in order to derive bounds from direct detection we will assume that for each point in the parameter space we are able to reproduce the DM abundance.

Irrespectively of the Stueckelberg nature of the complex dark photon, our limits should only be applied when $M \ll M_\star$, while we are free to vary g_\star from a weak to a moderate strong coupling regime, without invalidating the EFT approach. In what follows, we will always fix g_\star to two specific values (to be discussed below) and show bounds obtained fixing the value of the Wilson coefficients $d_i = 1$, $c_i = 1$, leaving M_\star free to vary, so that exclusion curves will thus be read as lower bounds on the size of M_\star . Clearly, the validity of the EFT requires that the new physics scale, *i.e.* the mass of the heavy mediator M_\star , must be much larger than the light complex dark photon degree of freedom. We here define for convenience the ratio

$$R \equiv \frac{M_\star}{M}, \quad (27)$$

in such a way that the EFT description is valid as long as $R \gg 1$. We will comment later on the effect of changing the value of g_\star . Each bound will be shown for both power counting schemes (naive and improved) discussed in sections 2.2 and 3.

We start our discussion in sec. 5.1 by discussing the limits coming from the invisible decays of the Higgs and Z bosons, and then in sec. 5.2 we will instead compute bounds coming from direct detection experiments, following the same prescription for the size of the Wilson coefficients.

5.1 Collider Constraints: Higgs and Z invisible decays

In this section we consider the effect of DM in the invisible branching ratios of Higgs and Z boson. As such, we are applying our EFT in an energy range where $M \ll E$ and our improved power counting has to be used. In order to show its effect on the limits, we present a comparison between what happens with and without such power counting fixing $g_\star = 1$.

When the Higgs and Z bosons are heavier than twice the DM mass, all dimension 4 operators in eq. (15) and some of the effective operators in eq. (16) may induce their decay into a particle-antiparticle pair of DM. We can then use the measured value of the decays into invisible states to put bounds on

Operators	Coefficients α_i	Kinematic factor η_i
$V_\mu \bar{V}^\mu (H ^2, H ^4)$	$\alpha_1 = \left[1, \frac{M^2}{M_*^2}\right] g_*^2 v (d_H + c_H \frac{g_*^2 v^2}{M_*^2})$	$\eta_1 = \frac{(M_h^2 - 2M^2)^2}{4M^4} + 2$
$V_{\mu\nu} \bar{V}^{\mu\nu} H ^2$	$\alpha_2 = \frac{g_*^4}{16\pi^2} c_{H,2} \frac{v}{M_*^2}$	$\eta_2 = 2M^4 \left(6 - 4\frac{M^2}{M_h^2} + \frac{M_h^4}{M^4}\right)$
$\tilde{V}_{\mu\nu} \bar{V}^{\mu\nu} H ^2$	$\alpha_3 = \frac{g_*^4}{16\pi^2} c_{H,3} \frac{v}{M_*^2}$	$\eta_3 = 8M_h^4 \left(1 - 4\frac{M^2}{M_h^2}\right)$
$V_{(\mu} \bar{V}_{\nu)} \partial^{(\mu} \partial^{\nu)} H ^2$	$\alpha_4 = \left[1, \frac{M^2}{M_*^2}\right] c_{D2H} \frac{g_*^2 v}{2M_*^2}$	$\eta_4 = \frac{M_h^4 (M_h^2 - 4M^2)^2}{4M^4}$

Table 6. List of the parameters appearing in the invisible decay width of the Higgs boson, see eq. (28a). For each set of parameters we also present the operator(s) that generate them. We also show in square brackets the two alternative solutions for the naive and improved power counting when a choice is needed.

Operators	Coefficients β_i	Kinematic factor ρ_i
$J_\mu^V J_H^\mu$	$\beta_1 = \left[1, \frac{M^2}{M_*^2}\right] \sqrt{g^2 + g'^2} c_{Hc} \frac{g_*^2 v^2}{2M_*^2}$	$\rho_1 = \frac{M_Z^6 - 8M^2 M_Z^4 + 28M^4 M_Z^2 - 48M^6}{12M^4}$
$J_\mu^P J_H^\mu$	$\beta_2 = \left[1, \frac{M^2}{M_*^2}\right] \sqrt{g^2 + g'^2} c_{\tilde{H}c} \frac{g_*^2 v^2}{2M_*^2}$	$\rho_2 = \frac{(M_Z^2 - 4M^2)^2}{3M^2}$
$V_{[\mu} \bar{V}_{\nu]} B^{\mu\nu} (1, H ^2)$	$\beta_3 = \left[1, \frac{M^2}{M_*^2}\right] \frac{g_*^2 g'}{16\pi^2} s_{\theta_w} (d_B + c_{HB} \frac{g_*^2 v^2}{2M_*^2})$	$\rho_3 = \frac{M_Z^2}{12} \left(\frac{M_Z^4}{M^4} - 16\right)$
$V_{[\mu\rho} \bar{V}_{\nu]}^{\rho} B^{\mu\nu}$	$\beta_4 = \frac{g_*^2 g'}{16\pi^2} s_{\theta_w} \frac{c_B}{M_*^2}$	$\rho_4 = \frac{M_Z^4}{6} \left(M_Z^2 - 8\frac{M^4}{M_Z^2} - 2M^2\right)$
$V_{[\mu} \bar{V}_{\nu]} \tilde{B}^{\mu\nu} (1, H ^2)$	$\beta_5 = \left[1, \frac{M^2}{M_*^2}\right] \frac{g_*^2 g'}{16\pi^2} s_{\theta_w} (d'_B + c_{HB'} \frac{g_*^2 v^2}{2M_*^2})$	$\rho_5 = \frac{1}{3} \left(\frac{M_Z^4}{M^2} + 2M_Z^2\right)$
$V_{[\mu\rho} \bar{V}_{\nu]}^{\rho} \tilde{B}^{\mu\nu}$	$\beta_6 = \frac{g_*^2 g'}{16\pi^2} s_{\theta_w} \frac{c'_B}{M_*^2}$	$\rho_6 = \frac{2}{3} M_Z^4 \left(1 - 2\frac{M^2}{M_Z^2} + 4\frac{M^4}{M_Z^4}\right)$

Table 7. As in table 6 but for the $Z \rightarrow V\bar{V}$ decay, see eq. (28b). The couplings g and g' are the usual $SU(2)_L \times U(1)_Y$ gauge couplings, while s_{θ_w} is the sine of the weak angle.

the parameter space of the EFT we are considering. We write the two relevant decay widths as

$$\Gamma_{h \rightarrow V\bar{V}} = \frac{1}{16\pi M_h} (\sum_i |\alpha_i|^2 \eta_i) \sqrt{1 - \frac{4M^2}{M_h^2}}, \quad (28a)$$

$$\Gamma_{Z \rightarrow V\bar{V}} = \frac{1}{16\pi M_Z} (\sum_i |\beta_i|^2 \rho_i) \sqrt{1 - \frac{4M^2}{M_Z^2}}, \quad (28b)$$

where M_h and M_Z are the Higgs and Z bosons masses, respectively. The values of the coefficients α_i , β_i , and the kinematic structures η_i and ρ_i are collected in tables 6 and 7, together with the operators that generate the decays. For the coefficients α_i and β_i we show in brackets the two alternative choices associated with the naive and improved power counting solutions. To obtain the value of the coefficient in the naive power counting scheme, it is sufficient to set to unity the content of the square bracket.

We have written the decay widths in this form to highlight two effects. First, the coefficients α_i and β_i are just avatars for the Wilson coefficients of eq. (14), and as such they are linear in them, as can be seen from tables 6 and 7. Second, the coefficients ρ_i and η_i are instead kinematic factors, that only depend on M , and they differ from case to case. In particular, by looking at table 6 and table 7, we see that they might display apparent divergences as $M \ll M_{h,Z}$. This makes self-evident the situation that might arise by extrapolating bounds fixing α_i, β_i and letting M drops arbitrarily.

Assuming that the decay into the $V\bar{V}$ pair saturates the h and Z invisible widths, we can set bounds

using the experimental values $BR_{h \rightarrow \text{inv}} < 13\%$ [72] and $\Gamma_{Z \rightarrow V\bar{V}} < \delta\Gamma(Z \rightarrow \text{inv})$, where $\delta\Gamma_{Z \rightarrow \text{inv}} = 1.5$ MeV is the error on the Z invisible width [72].

Our results are presented in Fig. 2 where we show the constraints for each operator in the plane (M, M_\star) . In such figure all the dimensionless coefficients are set to one, allowing us to display all the constraints in the same plot. On the left panels of figure 2 we show the limits on M_\star obtained using the naive power counting, while on the right panels we show the limits on M_\star obtained with the improved power counting. The upper and lower panels present the limits obtained from $h \rightarrow \text{inv}$ and $Z \rightarrow \text{inv}$, respectively.

We have included all the leading effect from the operators of eq. (14) with a caveat for the ones appearing in (15). Indeed, they do not show up in the naive power counting as they are 'renormalizable' and no power of M_\star appears in the naive scaling.

We also highlight the regions in which the validity of the EFT computation is questionable: the horizontal regions show when $M_\star < 5M_{h,Z}$ (light grey) or $M_\star < 10M_{h,Z}$ (dark grey), depending on the case considered, while the oblique regions refer to $R < 5$ (light blue) and $R < 10$ (lighter blue).

As it is clear from the left panels, when the naive power counting is used for the operators that do not contain the DM field strength and are, thus, not invariant under the dark gauge $U(1)_D$, the bounds become stronger as we move to lower values of M . Namely, the bound mass M_\star becomes larger and larger. This is due to the $1/M^4$ enhancement discussed in sec. 2.2 and it is cured once the improved power counting is used (see right panels). In the naive power counting case, this means that the bound grows less fast than for the other operators, while when the improved power counting is used, this means that the bound becomes irrelevant for small masses, *i.e.* as the decay width vanishes in the $M \rightarrow 0$ limit. The only exceptions are given by the non-gauge invariant CP-odd operators, associated to the Wilson coefficients $(\mathcal{C}'_{\tilde{H}c}, \lambda'_B, \mathcal{C}'_{HB})$. As can be seen from table 7, due to the presence of the Levi-Civita tensor in the operators, for $M \ll M_Z$ the decay width scales as M^{-2} (M^2) when the naive (improved) power counting is used.

In general we observe that the bounds obtained using the improved power counting are less constraining than those obtained using the naive power counting due to the additional $M^2/M_\star^2 \ll 1$ suppression. When using the improved power counting scheme, the choice $g_\star = 3$ allows us to have some of the limits falling into the region in which the validity of the EFT is not questionable. For lower values of g_\star , all the limits would fall in the excluded region. As such, colliders limits are then mostly applicable in EFT terms when the underlying model has some strong coupling.

The limits for different values of g_\star can be easily obtained from the ones shown in Fig. 2 by an appropriate rescaling. For instance, consider the bound on M_\star obtained switching on the operator $V_\mu \bar{V}^\mu |H|^4$, with coefficient $[1, M^2/M_\star^2]g_\star^4 c_H/M_\star^2$ as in eq. (16). The bound on M_\star can be written as

$$M_\star[M] \geq (M_\star[M])^{\text{bound}, g_\star=1} \begin{cases} g_\star^2 & \text{(naive)} \\ g_\star & \text{(improved)}, \end{cases} \quad (29)$$

where $(M_\star[M])^{\text{bound}, g_\star=1}$ is the experimental bound as a function of the DM mass obtained in a given power counting, that can be read from Fig. 2. The different dependence on g_\star in eq. (29) is due to the different dependence of the decay widths on M_\star in the two power counting schemes. For the remaining operators, it is now easy to repeat this reasoning considering the correct powers of g_\star and to obtain the bound for any value of the coupling.

This exercise shows that the bounds from invisible decays of H and Z are not so constraining as one might think. We show that this is especially true for a weakly coupled realization. From the right panels of figure 2 we see for example that also the 'Higgs portal' c_H is not so constraining once the

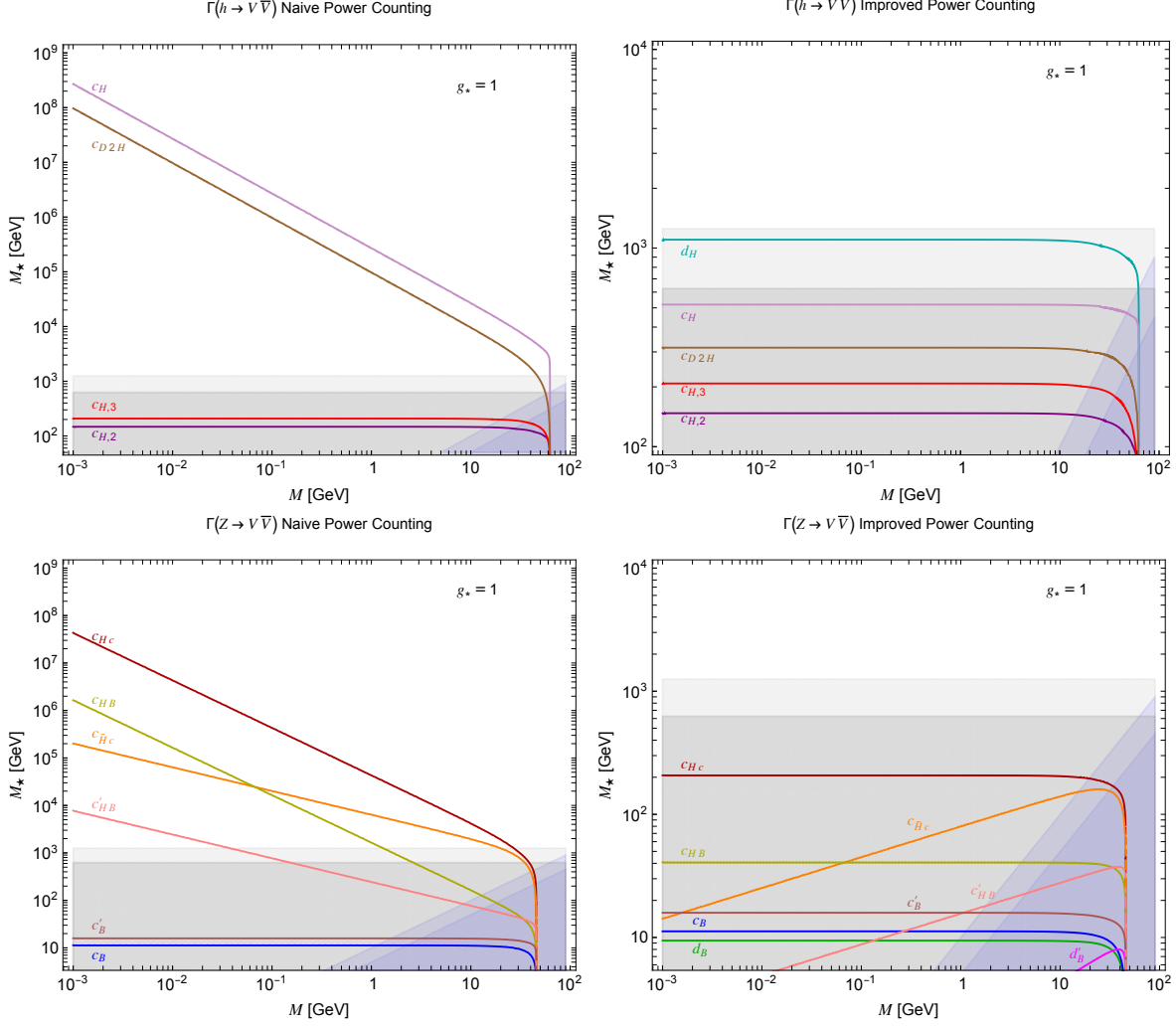


Figure 2. Regions excluded by the bound on the invisible decays of the Higgs boson (upper panels) or Z boson (lower panels). The regions excluded are those below the colored lines. In the left (right) panel we show the limits obtained using the naive (improved) power counting. All the limits are obtained fixing $g_\star = 1$, $d_i = 1$ and $c_i = 1$. The grey horizontal regions show when $M_\star < 5M_{h,Z}$ or $M_\star < 10M_{h,Z}$, while the oblique lines show the regions in which $R < 5$ (lightblue) or $R < 10$ (lighter blue).

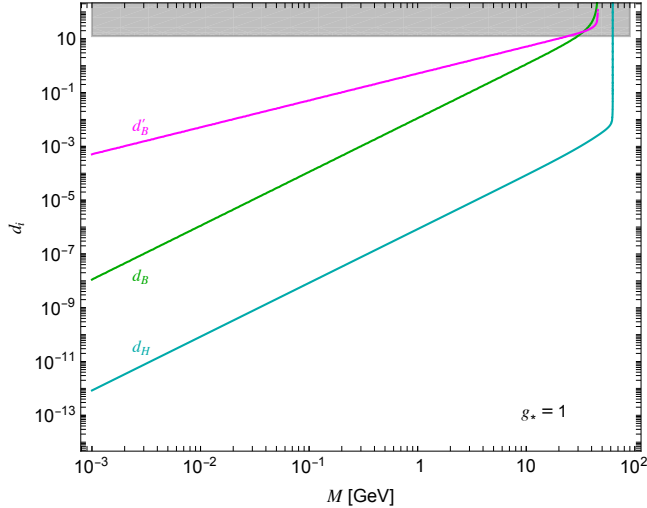


Figure 3. Upper limits on the (d_h, d_B, d'_B) coefficients, corresponding to the Wilson coefficients of renormalizable operators in eq.(15) when the naive power counting is used. The curves are obtained for $g_* = 1$ and represent the constraints obtained from Higgs and Z bosons invisible decay modes.

improved power counting is applied. This is also what happens in explicit realizations and we believe it is the right way to inspect EFT of dark photon dark matter.

As a final remark we show the bounds on the quartic couplings c_H and $c_B^{(\prime)}$ when the naive power counting is used in Fig. 3, where the constraints live in the plane $(M, \text{couplings})$. For c_H , this is the usual bound on the Higgs portal coupling [15, 17, 45–50], while the $c_B^{(\prime)}$ coupling has been studied in the context of the coupling between vector DM and electromagnetic and weak multipoles [61, 62]. In this case, the grey shaded region is drawn in correspondence of the benchmark value $c_i \geq 4\pi$, which is the typical value for breakdown of perturbativity and unitarity.

Summary of collider searches

Our procedure has identified a selection of operators that are mostly constrained by invisible decays of H and Z . As discussed, the bounds are not important for a theory of weakly coupled complex dark photon ($g_* = 1$) when we apply the correct power counting solution (fig. 2), i.e. the *improved* one (see sec. 3.1). Since they apply in a region beyond the EFT valid.

In figure 4 we can appreciate that only the operators connected with the Higgs invisible decay mode happen to escape the regions where the validity of the EFT breaks down as the requirement on the separation of scales fails. In this case, the well known Higgs portal operator d_H (*dark cyan* line) sets the largest lower bound on the new physics scale M_* and would therefore be relevant for the effective theory phenomenology. Other relevant exclusion regions in this scenario are given by $(c_H, c_{H,2}, c_{H,3})$ which are the dimension six Higgs portal, the CP-even and CP-odd field strength operators, respectively. As a reference, we also show that the strongest bound from $Z \rightarrow \text{inv}$ associated to the *dark red* line still cannot overcome the EFT validity region.

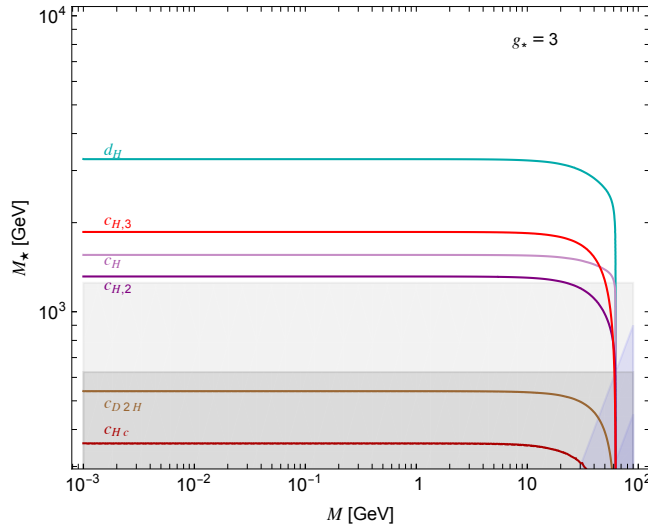


Figure 4. Bounds on the parameters space (M, M_*) from invisible decay of H and Z bosons. Each line correspond to the Wilson coefficient of the EFT as in table 6. We show the constraints arising from one operator at a time, and the region below each curve is excluded. The results apply for $g_* = 3$ with all the dimensionless coefficients $d_i, c_i = 1$ when the *improved* power counting is used. Shaded regions correspond to regions of parameters space where the EFT validity breaks down: $M_* \leq (5, 10)M_h$ in grey and $R \leq [5, 10]$ in light blue.

5.2 Direct Detection

In this section we describe how direct detection experiments can put bounds on the parameter space of the EFT we are considering. Despite direct detection experiment work at low energy transfer, therefore in a regime where the non-renormalizable nature of massive vector does not appear, we find that the power counting developed in the previous section still provides a suppression to otherwise unphysical large effects in the rates. The bounds derived here connects with the discussion of sec. 4.

As already mentioned in that section, we consider only spin-independent bounds, which should impose the stronger constraints on our model. The relevant Lagrangian we consider is the one in eq. (25), with Wilson coefficients given in eq. (26). As can be seen with our derivation, the EFT Lagrangian of eq. (14) generates only six non-relativistic spin-independent operators

$$\text{direct detection : } (\mathcal{O}_1^{\text{NR}}, \mathcal{O}_5^{\text{NR}}, \mathcal{O}_8^{\text{NR}}, \mathcal{O}_{11}^{\text{NR}}, \mathcal{O}_{17}^{\text{NR}}, \mathcal{O}_{19}^{\text{NR}}), \quad (30)$$

and we refer again to table 5 for the definitions. We focus on these in the remainder of this section. Naively one would expect that $\mathcal{O}_1^{\text{NR}}$ would give the strongest constraint, but the results would be radically different when low-momentum enhancement are considered.

In order to set the limits coming from direct detection experiments, we use the following approximate procedure. We use the 95% C.L. exclusion obtained by the LZ experiment on the DM-nucleon spin-independent cross section [73] and plug it inside eq. (59) to obtain the number of experimentally excluded events $N_{\text{exp}}(M)$ as a function of the DM mass. For this computation, we use the Helm form factor as nuclear response function representative of the spin-independent search. For each of the Wilson coefficients appearing in eq. (15) and eq. (16), we then compute the number of events

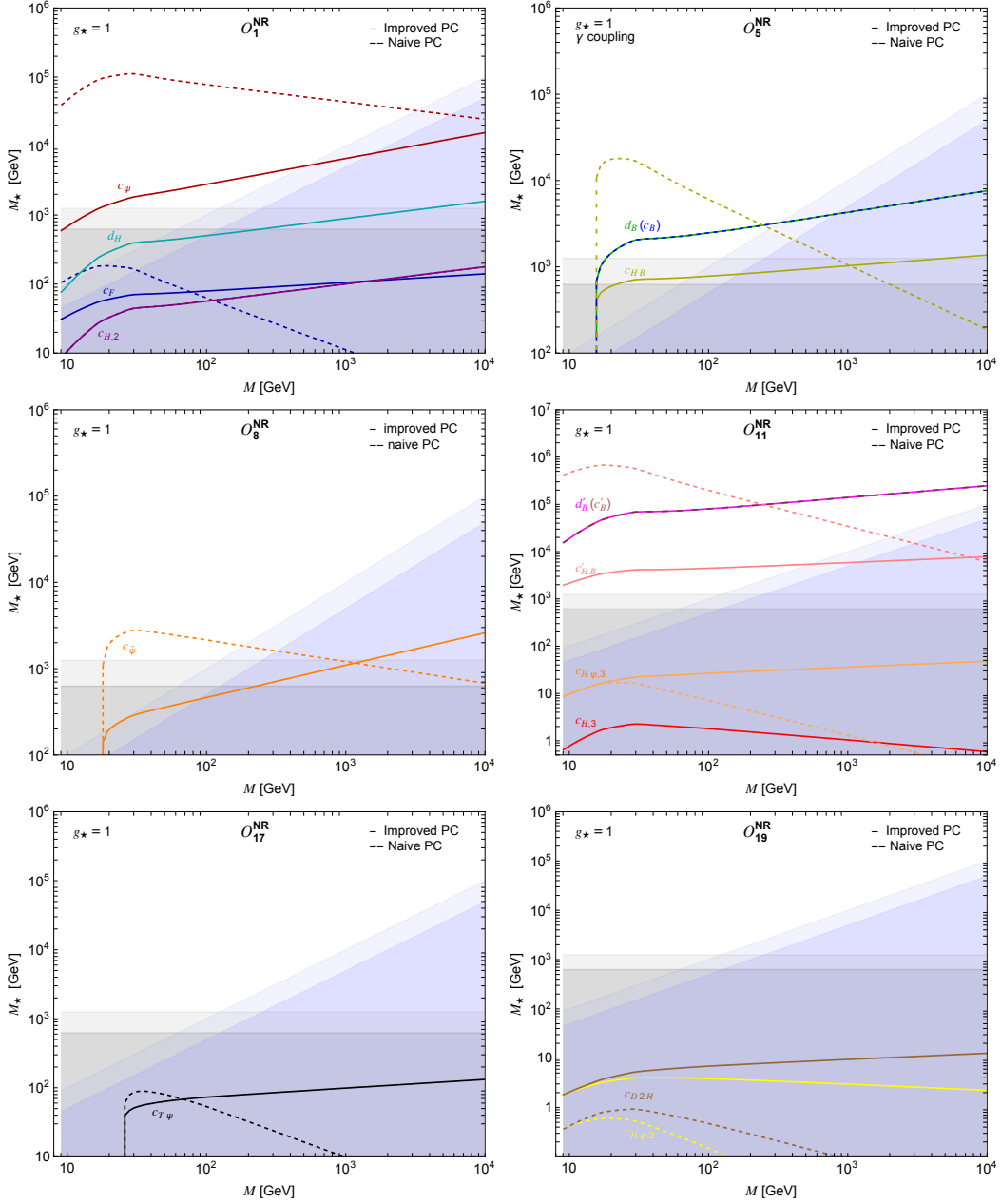


Figure 5. Lower bounds on the new physics scale M_* derived for each operator $\mathcal{O}_i^{\text{NR}}$ contribution to our ”reduced” SI NREFT describing a complex dark photon undergoing elastic scattering off nuclei. We compare the constraints derived adopting both the naive (*dashed lines*) and the improved (*solid lines*) power counting solutions. All curves are plotted for the benchmark value $g_* = 1$. *Grey* and *lightblue* shaded regions correspond to parameters space patches where the EFT validity is questionable, i.e. when $M_* \leq (5, 10)M_h$ and $R = M_*/M \leq (5, 10)$ respectively.

$N_{\text{model}}(M; \{\mathcal{C}_i, g_\star, M_\star\})$, following all the matching procedure and the computation of the cross section as explained in appendix B. We obtain the excluded region imposing

$$N_{\text{model}}(M; \{\mathcal{C}_i, g_\star, M_\star\}) < N_{\text{exp}}(M). \quad (31)$$

More details on the computation of the number of events at direct detection experiments can be found in appendix B.

Our results are presented in Fig. 5, where we show a comparison between the limits obtained using the naive (dashed lines) and improved (solid lines) power counting in the plane (M, M_\star) . Each panel shows one of six different non-relativistic operators generated when matching onto the NREFT of eq. (25) as discussed in sec. 4. Shaded regions are the same as in Fig. 2 and show the regions in which the EFT is not a valid expansion anymore. In all the plots the dimensionless coefficients d_i, c_i are set to unity. For each line $M_\star(M)_{\text{excl.}}$, the excluded region stays below that line.

In discussing our surveys of bounds, two main points have to be considered. First, we see that the improved power counting strongly relaxes the bound in the EFT regime (when $R \gg 1$), since in all the plots the solid line stay below the dashed line of corresponding color. Second, some non-relativistic operators are enhanced by inverse powers of q^2 , which may overcome the suppression of q and v at the numerators. This fact allows us to explain why the bound on $M_\star(M)$ from $\mathcal{O}_1^{\text{NR}}$ is comparable to the bound arising from $\mathcal{O}_{5,11}^{\text{NR}}$. The operator $\mathcal{O}_1^{\text{NR}}$ is the only NR interaction not suppressed by powers of DM velocity or exchanged momentum. However, we obtain physically significant bounds also from $\mathcal{O}_{11}^{\text{NR}} = i(\vec{q} \cdot \vec{S}_V)/m_N$ (that carries one factor of the exchanged momentum \vec{q}), and from $\mathcal{O}_5^{\text{NR}} = i\vec{S}_V \cdot (\vec{q} \times \vec{v}_\perp)/m_N$ (further suppressed by one factor of \vec{v}_\perp). These results could appear quite surprising, but they are easily explained remembering that, despite the $\sim q, \sim qv_\perp$ suppression, both Wilson coefficients of these NR operators receive leading order contributions in a q^n expansion from the magnetic and electric "dipole-like" interactions

$$\{V_{[\mu}\bar{V}_{\nu]}B^{\mu\nu}, V_{[\mu\rho}\bar{V}_{\nu]}B^{\mu\nu}, V_{[\mu}\bar{V}_{\nu]}\tilde{B}^{\mu\nu}, V_{[\mu\rho}\bar{V}_{\nu]}\tilde{B}^{\mu\nu}\},$$

that are labelled by coefficients $\lambda_B^{(\prime)}, c_B^{(\prime)}$ as in eq. (18) and table 3. This results in a $1/\vec{q}^2$ enhancement factor typical of the long range interaction at low exchanged momentum, so that we obtain a significant bound in a region in which the EFT is valid. In particular we point out that complex dark photon DM is the only scenario where a dimension-4 operator - although cured by the improved power counting - can give rise to an electric dipole moment interaction, corresponding to $q^{-2}\mathcal{O}_{11}^{\text{NR}} = q^{-2}i(\vec{q} \cdot \vec{S}_V)/m_N$, therefore giving a low-momentum enhancement which is unsuppressed by the DM velocity (contrary to the magnetic dipole interaction, which is still suppressed by v).

In terms of the naive power counting rule we can impose upper limits on the coefficients of the four operators of (15). The results are shown in Fig. 6.

Before concluding, it is worth emphasizing that half of the bounds on the NR operators bounds do not extend over the whole mass range investigated by the LZ experiment, with the curves terminating abruptly, rather than smoothly. This feature can be traced to their \vec{q}, \vec{v}_\perp dependence. These enter the calculation of the total number of theoretically expected events through the velocity (astrophysical uncertainty) and recoil energy (experimental input) integrated form factor discussed in eq. (57) of Appendix B, which is (partially) responsible of the shape and responsible of the fact that they close earlier than the experimental window.

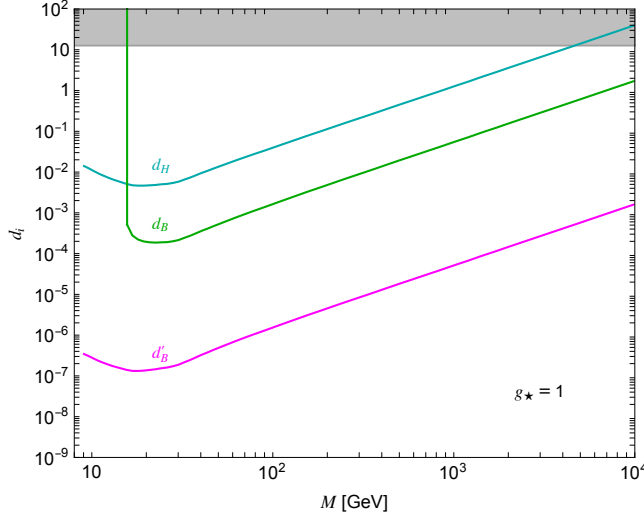


Figure 6. Upper limits on the (d_h, d_B, d'_B) coefficients, corresponding to the Wilson coefficients of renormalizable operators in eq.(15) when the naive power counting is used. The curves are obtained for $g_\star = 1$ and represent the constraints obtained from spin-independent direct detection at LZ.

Summary of direct detection

Our procedure has identified a selection of operators that are mostly constrained by direct detection. In figure 7 we focus on the resulting exclusion curves $M_\star(M)$ obtained for a weakly coupled dark sector $g_\star = 1$ when the correct behaviour of effective operators under gauge transformations is restored applying the *improved* power counting (see sec. 3.1). All curves correspond to $d_i, c_i = 1$.

We notice that the exclusion of a few interactions (as for example the Higgs portal d_H , *dark cyan* line) fall in a region beyond the EFT validity. We conclude that Higgs portal phenomenology is not so relevant for vector DM (see however [17]).

However, other operators receive meaningful exclusion limits in a region where the EFT is fully valid. This is the case for dipole-like operators corresponding to $d_B^{(i)}, c_B^{(i)}$ and c'_{HB} . They provide the strongest lower bounds on the new physics scale $M_\star(M)$ even for moderate couplings $g_\star = 1$. This was already noticed in [62] that used previous Xenon data. For complex vectors the most interesting channel is the one mediated by electric-dipole interaction with the photons $\mathcal{O}_{\mu\nu}^A \tilde{F}^{\mu\nu}$ corresponding d'_B . In the NREFT it receives a $1/\bar{q}^2$ enhancement at low momentum transfer – typical of long-range interactions mediated by the photon – and no v suppression that set $M_\star(M) \gtrsim 10^4 - 10^5$ GeV throughout the investigated mass window. It gives a strong bound even with the improved power counting.

5.3 Massless Stueckelberg case

In section 3.2 we briefly discussed the possibility that the physical complex dark photon mass is completely generated by the EFT operators, once we set $M = 0$. Considering only the leading effect coming from the Wilson coefficient λ_H , we would have that the dark photon mass equals

$$m_V^2 = d_H g_\star^2 \frac{v^2}{2}, \quad (32)$$

i.e. fixed by the coefficient d_H . In this case, we can then study when collider and direct detection bounds can place constraints on such a scenario. We show our results in fig. 8. In both panels, the

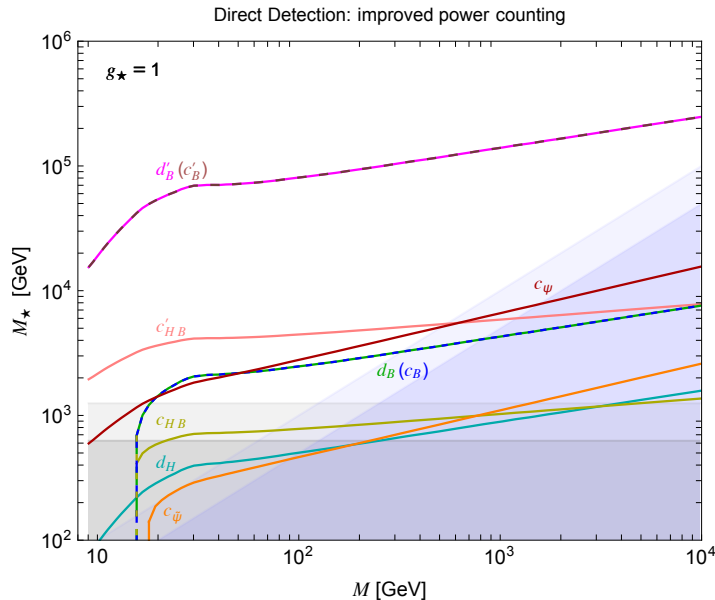


Figure 7. Bounds on the parameters space (M, M_*) from spin independent direct detection at LZ. Each line correspond to the Wilson coefficient of the EFT as in table 5. We show the constraints arising from one operator at a time, and the region below each curve is excluded. The results apply for $g_* = 1$ with all the dimensionless coefficients $d_i, c_i = 1$ when the *improved* power counting is used. Shaded regions correspond to regions of parameters space where the EFT validity breaks down: $M_* \leq (5, 10)M_h$ in grey and $R \leq [5, 10]$ in light blue.

dashed line represents the dark photon mass of eq. (32). On the left panel, the experimental bound is the one obtained from the Higgs decay width, while on the right panel is the one obtained from LZ. As we can see, the limit coming from the Higgs decay width exclude this scenarios for masses below $M_h/2 \simeq 63$ GeV. On the other hand, the limits coming from the LZ experiment exclude the scenario for masses above $(14 - 15)$ GeV, meaning that this simple scenario is completely excluded. We observe that the conclusion is independent on the value of g_* , since the experimental limits and the dark photon mass scale in the same way once we allow for $g_* \neq 1$.

6 Sketching possible UV completions

In this section we present two explicit UV complete models that generate, under some assumptions about hierarchy of vacuum expectation values, some of the operators that appear in the low energy EFT of a complex dark photon. In our discussion, we pay special attention to the requirements necessary to generate the improved and the naive power counting described in Sec. 3.1.

6.1 Model I: $SU(2) \times U(1)$

The first model we present is based on a $SU(2) \times U(1)$ dark gauge symmetry (see also Refs. [51, 57–59, 62, 74]), completely broken by the vacuum expectation values (vevs) of two scalars transforming as $\phi \sim (\mathbf{d}, q)$ and $\varphi \sim (\mathbf{1}, q')$. Here \mathbf{d} denotes a generic dimension- d representation of $SU(2)$ and q, q' are the $U(1)$ charges. Both scalars are complete singlets under the SM gauge group. We denote by

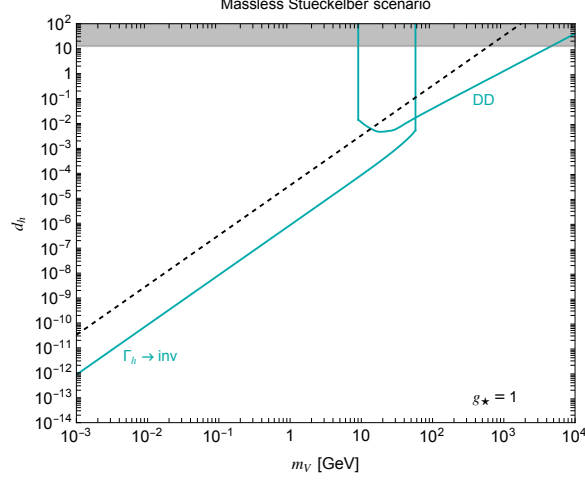


Figure 8. Limits coming from the Higgs invisible BR and DD searches on the scenario. The dashed line represents the values of parameters in which eq. (32) is satisfied, namely in which the dark photon mass is completely generated by contact interactions between DM and SM fields (more specifically, by the d_H coefficient).

V^a and X the gauge bosons of SU(2) and U(1), respectively, with corresponding gauge couplings g_D and g'_D . The DM candidate V and its antiparticle are given by the combinations $V = (V^1 - iV^2)/\sqrt{2}$ and $\bar{V} = (V^1 + iV^2)/\sqrt{2}$. As we are now going to show, the EFT generated integrating out the heavy scalar and vector states will include the Higgs portal interactions, as well as vector \times vector and tensor \times tensor operators.

For what concerns the generation of effective operators via scalar exchange, the relevant interactions are contained in the following potential

$$V(\phi, \varphi, H) = -\mu_\phi^2 |\phi|^2 + \lambda_\phi |\phi|^4 - \mu_\varphi^2 |\varphi|^2 - \lambda_\varphi |\varphi|^4 - \lambda_1 |\phi|^2 |\varphi|^2 - \lambda_2 |\phi|^2 |H|^2 - \lambda_3 |\varphi|^2 |H|^2, \quad (33)$$

that contains all the terms involving ϕ , φ and their interactions with the Higgs doublet H . In what follows, we will always consider scenarios for which

$$\langle \varphi \rangle \gg \langle \phi \rangle, \langle H \rangle, \quad (34)$$

in such a way that the mixing between ϕ and φ , that generates the *Higgs portal*, is given by

$$\theta_{\varphi\phi} \simeq \frac{\lambda_1 \langle \phi \rangle}{\lambda_\varphi \langle \varphi \rangle}. \quad (35)$$

Similarly, the kinetic mixing ε between $U(1)_Y$ and U(1) induces a mixing between the dark gauge bosons V^3 , X and the SM Z_{SM} and generates a *vector portal* between the dark and visible sector. After symmetry breaking, we can write the dynamical fields V^3 , X and Z_{SM} in terms of the mass eigenstates Z' , D and Z as follows:

$$\begin{cases} V^3 \simeq Z' + \theta_{XV^3} D + \dots \\ X \simeq D - \theta_{XV^3} Z' - \theta_{XZ} Z_{SM} + \dots \\ Z \simeq Z_{SM} + \theta_{XZ} D + \dots \end{cases} \quad \begin{cases} \theta_{XV^3} \simeq \frac{q g'_D}{m \sqrt{1-\varepsilon^2} g_D} \frac{M^2}{M_X^2}, \\ \theta_{XZ} \simeq \frac{\varepsilon g'}{g_Z \sqrt{1-\varepsilon^2}} \frac{M_Z^2}{M_X^2}, \end{cases} \quad (36)$$

where we have written the expansion for the mixing angles. The vector masses are

$$M = g_D \langle \phi \rangle \sqrt{\ell(\ell+1) - m^2}, \quad M_{Z'} \simeq m g_D \langle \phi \rangle, \quad (37)$$

$$M_D \simeq \frac{g'_D q'}{\sqrt{1-\varepsilon^2}} \langle \varphi \rangle, \quad M_Z \simeq M_{Z_{\text{SM}}}, \quad (38)$$

where $\ell = (d-1)/2$ and $m = -\ell, \dots, +\ell$ are the usual $SU(2)$ quantum numbers (m labels the direction along which the vev is aligned [29]).

We now focus on the generation of the EFT. For the moment, we do not assume any hierarchy between $\langle \phi \rangle$ and $\langle H \rangle$, so that the only heavy states are those whose masses are $\mathcal{O}(\langle \varphi \rangle)$, *i.e.* $D \simeq X$ and φ . The operator $V_\mu \bar{V}^\mu |H|^2$ is generated by the scalar portal once φ is integrated out. We obtain

$$\mathcal{M}_{V\bar{V}H^\dagger H}^{(\varphi)} = g_{\varphi V\bar{V}} \frac{1}{M_\varphi^2} g_{\varphi H^\dagger H} \epsilon_V \epsilon_{\bar{V}} \sim \frac{\lambda_1 \lambda_3}{\lambda_\varphi} \frac{M^2}{M_\varphi^2} \epsilon_V \epsilon_{\bar{V}}, \quad \text{with } \frac{\lambda_1 \lambda_3}{\lambda_\varphi} \sim g_\star^2, \quad (39)$$

where $\epsilon_V \epsilon_{\bar{V}}$ denote, schematically, the DM polarization vectors and we have used that the coupling between φ and the $V\bar{V}$ pair goes like $g_{\varphi V\bar{V}} \sim (M^2/\langle \phi \rangle) \theta_{\varphi\phi}$, while the coupling between φ and $H^\dagger H$ scales as $g_{\varphi H^\dagger H} \sim \lambda_3 \langle \varphi \rangle$. As we see, the Wilson coefficient obeys the ‘‘improved’’ power counting of Sec. 2.2, once we identify $M_\star \sim M_\varphi$.

Turning now to the current \times current operator $J_V^\mu J_\mu^B$, this is generated via the vector portal once we integrate out the heavy X state. We obtain (up to numerical factors)

$$\mathcal{M}_{V\bar{V}J_B}^{(X)} = g_{XV\bar{V}} \frac{1}{M_X^2} g_{XJ_B} \frac{1}{\sqrt{1-\varepsilon^2}} \epsilon_V \epsilon_{\bar{V}} \sim \frac{g'_D g' q \epsilon}{g_D} \frac{M^2}{M_X^4} \epsilon_V \epsilon_{\bar{V}}, \quad \text{with } \frac{g'_D g' q \epsilon}{g_D} \sim g_\star^2, \quad (40)$$

where we have used $g_{XV\bar{V}} \sim g_D \theta_{V^3 X}$, $g_{XJ_B} \sim g' \epsilon$, while the mixing angle can be found in eq. (36). Once again, we appreciate that the naive power counting $1/M_\star^2 = 1/M_X^2$ is corrected by the factor M^2/M_\star^2 , *i.e.* the ‘‘improved’’ power counting applies. Qualitatively similar results hold when we make the further assumption and consider $\langle \varphi \rangle \gg \langle \phi \rangle \gg \langle H \rangle$. For instance, if we consider the amplitude with a (now heavy) ϕ exchange, we obtain

$$\mathcal{M}_{V\bar{V}H^\dagger H}^{(\phi)} = g_{\phi V\bar{V}} \frac{1}{M_\phi^2} g_{\phi H^\dagger H} \epsilon_V \epsilon_{\bar{V}} \sim g_D^2 \frac{\lambda_2}{\lambda_\phi} \sqrt{\ell(\ell+1) - m^2} \epsilon_V \epsilon_{\bar{V}} \sim \frac{M^2}{M_\phi^2} \lambda_2 \epsilon_V \epsilon_{\bar{V}} \quad \text{with } \lambda_2 \sim g_\star^2. \quad (41)$$

Once more, we obtain the improved power counting we have advocated for in the text.

We conclude observing that the $SU(2)$ non-abelian kinetic term contains, in addition to the $V_\mu^3 J_V^\mu$ coupling between V^3 and the DM vector current, also the tensor coupling $V_{\mu\nu}^3 V^{[\mu} \bar{V}^{\nu]}$. This means that the argument outlined above for the current \times current operators can be immediately extended to the tensor \times tensor operators generated through this term – *e.g.* the dipole-like contact term in the effective theory of eq. (15) – with the same conclusions about the power counting applying.

6.2 Model II: $SU(2)_L \times SU(2)_R \times \mathbb{Z}_2$

The second model we consider is based on a $SU(2)_L \times SU(2)_R \times \mathbb{Z}_2$ gauge symmetry. This time, the DM candidate only interacts with the visible sector via a Higgs portal since, being the dark gauge symmetry non-abelian, there is no kinetic mixing between the dark and visible sectors forbidding any interaction mediated by vector bosons. For concreteness, we denote by $V_{L,R}^a$ and $g_{L,R}$ the gauge bosons and

couplings of $SU(2)_{L,R}$. The symmetry is completely broken in two steps: first to $U(1)_L \times U(1)_R \times \mathbb{Z}_2$ by the vev of two triplets, $\Sigma_L \sim (\mathbf{3}, \mathbf{1})$ and $\Sigma_R \sim (\mathbf{1}, \mathbf{3})$; then to \mathbb{Z}_2 by the vev of two doublets, $\phi_L \sim (\mathbf{2}, \mathbf{1})$ and $\phi_R \sim (\mathbf{1}, \mathbf{2})$. The \mathbb{Z}_2 symmetry acts as

$$(\mathbb{Z}_2) \quad V_L^a \leftrightarrow V_R^a, \quad \Sigma_L \leftrightarrow \Sigma_R, \quad \phi_L \leftrightarrow \phi_R. \quad (42)$$

Invariance under dark parity transformation forces the equality between the gauge couplings $g_L = g_R \equiv g_d$, between the triplets vevs $\langle \Sigma_L \rangle = \langle \Sigma_R \rangle \equiv \langle \Sigma \rangle$ and between the doublets vevs $\langle \phi_L \rangle = \langle \phi_R \rangle \equiv \langle \phi \rangle$. The two-step symmetry breaking described above can be achieved assuming a hierarchy between dark scalar vevs $\langle \Sigma \rangle \gg \langle \phi \rangle$ and that the triplets vevs are aligned along the $\sigma^3/2$ generator. Under these hypothesis, the states $V_{L,R}^\pm = (V_{L,R}^1 \mp iV_{L,R}^2)/\sqrt{2}$ and the scalar triplets have $\mathcal{O}(\langle \Sigma \rangle)$ masses, while $V_{L,R}^3$ and the scalar doublet are much lighter, with masses of order $\mathcal{O}(\langle \phi \rangle)$. However, because of the \mathbb{Z}_2 symmetry, V_L^3 and V_R^3 are degenerate, so that we can identify our DM candidate via $V = (V_L^3 - iV_R^3)/\sqrt{2}$. Unlike what happened in the $SU(2) \times U(1)$ model, we have now successfully obtained a hierarchy between the mass of the DM and of the remaining states in the gauge multiplet without invoking large $SU(2)$ representations. The price we pay is the absence of the vector portal. The scalar portal operator is now obtained integrating out the heavy triplets instead of φ . The amplitude we obtain is the same as in eq. (39), with the identification $M_\varphi \rightarrow M_\Sigma$ and new, appropriate quartic coupling. Also in this case we thus have a situation in which the ‘‘improved’’ power counting is valid.

7 Conclusions

In this work, we have studied a scenario in which the dark matter candidate is a massive complex vector V_μ , dubbed *complex dark photon*. We assume that the spin-1 DM particle is the only low energy remnant of a more complex heavy dark sector with typical mass M_\star that, once integrated out, generates a set of effective operators that can be studied phenomenologically. The stabilization of the DM candidate is achieved via an accidental dark $U(1)_D$ symmetry which survives at low energy.

An essential point that must be highlighted is the fact that, in the EFT of a massive vector field, the power counting of the operators is subtler than the one of theories with spin-0 or spin-1/2 DM candidates. This is because the free theory of a massive Stueckelberg field is renormalizable, but this renormalizability is lost in general once interactions are turned on. In practice, this means that the theory may cease to be valid at an energy parametrically smaller than the naive cutoff M_\star . To correct this behavior and reinstate M_\star as cutoff of the EFT, we introduced the so-called ‘‘improved power counting’’, in which we replace $V_\mu \rightarrow (M/M_\star)V_\mu$.

We then turned to the main point of the paper, i.e. the construction of the EFT Lagrangian at the scale M_\star , considering operators up to dimension 6 and paying particular attention to the elimination of redundant operators. With this information, we studied the effective theories obtained at lower energies, having in mind applications in direct detection experiments. We first integrated out SM particles at the electroweak scale (Higgs, W and Z bosons and the top quark). We then moved to energies of order 1 GeV and matched the operators to a single-nucleon relativistic EFT. Finally, we matched onto the non-relativistic theory that can be used to compute nuclear response functions and, ultimately, the number of events expected at direct detection experiments.

With all this information at our disposal, we finally turned to the phenomenological analysis, with the aim of putting limits on the Wilson coefficients of the operators defined at the scale M_\star . We considered two types of processes: SM particle decays (more specifically, Higgs and Z boson decays)

and limits coming from direct detection, namely, from the LZ experiment. Turning on one Wilson coefficient at a time, we studied the regions in parameter space which are experimentally excluded. In order to show the artificially large bounds one would obtain without considering the improved power counting, we compare the limits obtained using this rescaling of the field with the so-called “naive” power counting, in which the Wilson coefficient has simply the M_\star dependence dictated by the dimensions of the operator. The difference is particularly relevant when we consider high energy observables (Higgs and Z decays): with the naive power counting the bounds grow larger and larger the smaller the DM mass is taken, while this effect is correctly avoided once the improved power counting is considered. At low energy (direct detection) we also observe interesting effects, as strong limits are obtained on two types of operators: the one typically related to spin-independent direct detection experiments that sees the coherent enhancement and those obtained by the exchange in the t-channel of a massless photon, which are enhanced (rather than suppressed) by the small momentum exchange. This second class of operators are the spin-1 analog of electric and magnetic dipole operators that appear for spin-1/2 DM. However we emphasize that complex vectors are the only one that can display very large electric/magnetic dipole moments.

Finally, we turned to the question: which kind of UV completions can generate the EFT we have constructed? We presented two theories in which V_μ emerges as a gauge boson. In both cases, we have shown explicitly how the improved power counting is obtained once heavy dark states are integrated out. Since the relevance of the bounds crucially depends on the power counting, it could be interesting in the future to explore more generic schemes that allows for an even bigger enhancement of the operators constructed with SM field strength and complex vector DM fields, even though the UV completion might be difficult to identify.

Acknowledgments

The work of EB is partly supported by the Italian INFN program on Theoretical Astroparticle Physics (TAsP), by “Fundação de Amparo à Pesquisa do Estado de São Paulo” (FAPESP) under contract 2019/04837-9, as well as by Brazilian “Conselho Nacional de Desenvolvimento Científico e Tecnológico” (CNPq). AT acknowledges partial support from MIUR grants PRIN No. 2017L5W2PT.

A Polarizations of massive vectors

Definitions and properties

In this section we collect useful formulas for the computation of matrix elements in the EFT of complex dark photon. The free Lagrangian of our massive vector can be read out from the first two terms of eq. (1). The equations of motion are given by

$$\partial_\mu V^{\mu\nu} + M^2 V^\nu = \partial^\nu (\partial_\mu V^\mu), \quad (43)$$

and correspond to the Klein Gordon equation when the condition $\partial_\mu V^\mu = 0$ is imposed upon the field. This selects three physical polarizations for V_μ , which we will denote by $\varepsilon_\mu^s(p)$. Going to Fourier space and writing the 4-momentum of the particle as $p^\mu = (E_p, \vec{p})$, we have that the polarization vectors satisfy $p^\mu \varepsilon_\mu^s = 0$ and $g_{\mu\nu} \varepsilon_s^\mu \varepsilon_{s'}^\nu = -\delta_{ss'}$, where as usual the index s can take values $s = \pm$ for the transverse degrees of freedom and $s = L$ for the longitudinal one. They can be constructed from \vec{p} as

follows:

$$\varepsilon_{\pm}^{\mu} = (0, \vec{\varepsilon}_{\pm}), \quad \varepsilon_L^{\mu} = \left(\frac{|\vec{p}|}{M}, \frac{E_p}{M} \frac{\vec{p}}{|\vec{p}|} \right), \quad (44)$$

where $\vec{\varepsilon}_{\pm} \cdot \vec{p} = 0$. A useful way of rewriting the above polarization vectors, suitable for taking the non-relativistic limit, can be found as follows. In the rest frame of the particle we have $k^{\mu} = (M, \vec{0})$, and in that frame the three polarizations (that can be chosen to be eigenvectors of rotations around an axis, conventionally taken to be z) are in the fundamental representation of the little group $\text{SO}(3)$. We can thus write $\varepsilon_s^{\mu}(k) = (0, \xi_s^i)$ and the 3-polarizations can be taken to be orthonormal, $\xi_s^{\dagger} \xi_t = \delta_{st}$, with $s, t = 1, 2, 3$. In a generic frame in which the particle has 4-momentum $p^{\mu} = (E_p, \vec{p})$, the polarization vectors are obtained as $\varepsilon_s^{\mu}(p) = D[L(p, k)]^{\mu}_{\nu} \varepsilon_s^{\nu}(k)$, where $L(p, k)$ is the Lorentz transformation on k such that $p^{\mu} = L(p, k)^{\mu}_{\nu} k^{\nu}$, while $D[L]$ is a suitable representation of L . For vectors $D[L] = L$, since they transform in the 4-dimensional representation. Therefore, the polarization in a generic frame can be written as

$$\varepsilon_s^{\mu}(p) = \left(\frac{\vec{p} \cdot \vec{\xi}_s}{M}, \vec{\xi}_s + \frac{(\vec{p} \cdot \vec{\xi}_s)}{M(E_p + M)} \vec{p} \right), \quad (45)$$

which clearly satisfies the relativistic condition $p_{\mu} \varepsilon_s^{\mu}(p) = 0$ for any value of $\vec{p} \cdot \vec{\xi}_s$. In particular, in the non-relativistic limit we can neglect terms of order p^2/M^2 , obtaining

$$\varepsilon_s^{\mu}(p)|_{\text{NR}} = \left(\frac{\vec{p} \cdot \vec{\xi}_s}{M}, \vec{\xi}_s \right) + \mathcal{O}\left(\frac{p^2}{M^2}\right). \quad (46)$$

In presence of two particles we have also $p' = p - q$

$$\varepsilon_s^{\mu}(p')|_{\text{NR}} = \left(\frac{\vec{p}' \cdot \vec{\xi}_{s'}}{M}, \vec{\xi}_{s'} \right) + \dots \quad (47)$$

The spin operator $J_{\sigma}(\hat{n})$ is well-defined around any generic axis \hat{n} and the 3-vectors $\vec{\xi}$ and $\vec{\xi}'$ are its eigenstates; more precisely, $J_{\sigma}(\hat{n})\xi_s = \sigma \xi_s$, with $\sigma = -1, 0, 1$.

It is important to observe that, since the structure $\xi_s^a \xi_{s'}^b$, that will appear in the scattering amplitudes, is obtained by the product of two $\text{SO}(3)$ fundamentals, it can as usual be decomposed under $\text{SO}(3)$ as $\mathbf{3} \times \mathbf{3} = \mathbf{5} + \mathbf{3}_A + \mathbf{1}$, with $\mathbf{5}$ symmetric and traceless, $\mathbf{3}_A$ antisymmetric and $\mathbf{1}$ a singlet (trace). Therefore we have

$$\bar{\xi}_{s'}^a \xi_s^b = \mathcal{S}_{s's}^{ab} - \frac{i}{2} \epsilon^{abc} S_{s's}^c + \frac{1}{3} \delta^{ab} \mathcal{I}_V. \quad (48)$$

The appearance of a symmetric tensor structure is typical of a spin-1 DM candidate and is not present for spin-1/2 candidates, since group theory dictates that $\mathbf{2} \times \mathbf{2} = \mathbf{3}_S + \mathbf{1}_A$.

In section 6.1 of ref. [71] a similar decomposition is carried out, without singling out the trace part from the symmetric combination. We stress, however, that our decomposition follows directly from the irreducible spin representations of the product of polarization vectors of massive vectors and is thus more natural from this point of view.

Massive vectors polarization bilinears

As mentioned above, the product $[\bar{\xi}_{s'}^a \xi_s^b]$ appears in the matrix elements of the elastic DM-nucleus scattering. In particular, the possible structures are the ones generated by the operators \mathcal{O}_S , \mathcal{O}_{FS} , \mathcal{O}_{PS} , $J_{\mu}^{V,P}$ and $\mathcal{O}_{\mu\nu}^{A,S,T}$ listed in table 1. To fix our notation, we will take the incoming DM particle

to have momentum p^μ and spin state ξ_s , while the outgoing DM particle has momentum p' and spin state $\xi_{s'}$:

$$\text{DM}(\xi_s, \vec{p}) + \text{SM}(\vec{k}, \dots) \rightarrow \text{DM}(\xi_{s'}, \vec{p}') + \text{SM}'(\vec{k}', \dots), \quad (49)$$

where DM is our complex dark photon V . We also remind the set of Galilean invariant quantities of eq. (24) which will be used in the following. We summarize in table 8 the non-relativistic expansion for the polarization vector bilinears generated by such interactions, where we stop the NR expansion at leading order in a q^n expansion. The few the extra terms appearing in tensor structures components are kept since they would induce NR contributions that are NLO for the single UV operator but of the same order of other effects at the level of NREFT. In fact, for instance, terms like $q^2(\mathcal{O}_{1,19}^{\text{NR}})$ that arise from the dipole-like interactions when $\mathcal{O}_{\mu\nu}^A$ is contracted with the hyper-charge field strength, are clearly NLO in a momentum expansion due to the $\propto q^2$ factor, but would be competing effects of the same order of similar contributions from other effective operators once we take into account the long-range enhancement.

On top of that, we provide all the useful tools for a more complete analysis, but we urge the reader to remind that we have been coherent with our purpose of investigating only the characteristic LO signature of each UV Wilson coefficient when discussing direct detection phenomenology.

Sum rules

In computing the squared amplitudes we often encounter the sum over the spin indices s and s' of initial states. We here list the relevant sum rules for spin-1 particles:

$$\begin{aligned} \sum_{s's} \vec{A} \mathcal{I}_V &= 3A, & \sum_{s's} A_a \mathcal{S}_{s's}^{ab} \mathcal{S}_{s's}^b &= 0, \\ \sum_{s's} A_a \mathcal{S}_{s's}^a &= 0, & \sum_{s's} A_a \mathcal{S}_{s's}^{ab} B_b C_c \mathcal{S}_{s's}^c &= 0, \\ \sum_{s's} (\vec{S}_{s's})^2 &= -6, & \sum_{s's} A_a \mathcal{S}_{s's}^{ab} B_b \delta_{s's} &= 0, \\ \sum_{s's} \varepsilon_{abc} \varepsilon_{ajk} A^b \mathcal{S}_{s's}^c B^j \mathcal{S}_{s's}^k &= -4\vec{A} \cdot \vec{B}, & \sum_{s's} A_a \mathcal{S}_{s's}^{ab} B_c \mathcal{S}_{s's}^{cb} &= \frac{5}{3} \vec{A} \cdot \vec{B}, \\ \sum_{s's} A_a \mathcal{S}_{s's}^a B_b \mathcal{S}_{s's}^b &= -2\vec{A} \cdot \vec{B}, & \sum_{s's} A_a \mathcal{S}_{s's}^{ab} B_b A_c \mathcal{S}_{s's}^{cd} B_d &= \frac{1}{2} A^2 B^2 + \frac{1}{6} (\vec{A} \cdot \vec{B})^2. \end{aligned} \quad (50)$$

B Cross sections for direct detection

We collect here useful equations to compute the rate of events at direct detection experiments. Given the NREFT of eq. (25), the squared amplitude at the nucleon level, averaged over DM and nucleon spin degrees of freedom, can be written as

$$\overline{|\mathcal{M}_N|^2} = \frac{1}{2S_V + 1} \frac{1}{2S_N + 1} \sum_{s',s} \sum_{r',r} \sum_{i,j} c_i^N c_j^{N'} \langle N_{s'} V_{r'} | \mathcal{O}_i^{\text{NR}} \mathcal{O}_j^{\text{NR}} | N_s V_r \rangle, \quad (51)$$

where r, r', s, s' are spin indices. From this matrix element we can compute the DM-nucleon scattering cross section as

$$\sigma_N = \frac{\mu_N^2}{16\pi M^2 m_N^2} \overline{|\mathcal{M}_N|^2}. \quad (52)$$

Structure	Polarization Bilinear
Scalar	
$O_S = V_\mu \bar{V}^\mu$	$-\mathcal{I}_V + \dots$
$O_{FS} = V_{\mu\nu} \bar{V}^{\mu\nu}$	$-2M^2 \mathcal{I}_V + \dots$
$O_{PS} = \varepsilon^{\mu\nu\rho\sigma} V_{\mu\nu} \bar{V}_{\rho\sigma}$	$-4M(i\vec{q} \cdot \vec{S}_V) + \dots$
Vector	
$J_\mu^V = V_\nu \overleftrightarrow{\partial}_\mu \bar{V}^\nu$	$\begin{cases} -2M \mathcal{I}_V + \dots & (\mu = 0) \\ +P_i \mathcal{I}_V + \dots & (\mu = i) \end{cases}$
$J_\mu^P = \varepsilon_{\mu\nu\rho\sigma} V_\nu \overleftrightarrow{\partial}^\rho \bar{V}^\sigma$	$\begin{cases} -i\vec{S}_V \cdot \vec{P} + \dots & (\mu = 0) \\ +2iMS_{V,i} + \dots & (\mu = i) \end{cases}$
Tensor	
$O_{\mu\nu}^A = V_{[\mu} \bar{V}_{\nu]}$	$\begin{cases} 0 & (\mu = 0, \nu = 0) \\ -\frac{1}{M} \left(q_a \mathcal{S}_{s's}^{ai} - \frac{i}{2} \varepsilon_{iac} P^a S_V^c + q_a \frac{\delta^{ai}}{3} \mathcal{I}_V \right) + \dots & (\mu = 0, \nu = i) \\ i\varepsilon_{ijk} S_V^k + \dots & (\mu = i, \nu = j) \end{cases}$
$O_{\mu\nu}^S = V_{(\mu} \bar{V}_{\nu)}$	$\begin{cases} \frac{1}{2M^2} \vec{S}_V \cdot (i\vec{q} \times \vec{P}) + \dots & (\mu = 0, \nu = 0) \\ -\frac{1}{M} \left(P_a \mathcal{S}_{s's}^{ai} + \frac{i}{2} \varepsilon_{iac} q^a S_V^c + \frac{\delta^{ai}}{3} P_a \mathcal{I}_V \right) + \dots & (\mu = 0, \nu = i) \\ 2 \left(\mathcal{S}_{s's}^{ij} + \frac{\delta^{ij}}{3} \mathcal{I}_V \right) + \dots & (\mu = i, \nu = j) \end{cases}$
$O_{\mu\nu}^T = V_{[\mu\rho} \bar{V}_{\nu]}^\rho$	$\begin{cases} 0 & (\mu = 0, \nu = 0) \\ -iM \varepsilon_{iab} q^a S_V^b + \dots & (\mu = 0, \nu = i) \\ iM^2 \varepsilon_{ijk} S_V^k + \dots & (\mu = i, \nu = j) \end{cases}$

Table 8. We summarize the full set of polarization bilinears generated by each operator structure appearing in our EFT for a massive complex vector DM. We classified the structures of bilinears accordingly, making clear the different components for vector and tensor structure.

In order to compute the squared matrix element for the DM-target nucleus scattering amplitude, we simply need to multiply by the normalization factor m_T^2/m_N^2 (where m_T is the target nucleus mass) that accounts for the $|N\rangle \rightarrow |T\rangle$ substitution and to replace the $\sum_{s',s} \sum_{r',r} \langle N_{s'} V_{r'} | \mathcal{O}_i^{\text{NR}} \mathcal{O}_j^{\text{NR}} | N_s V_r \rangle / (2S_V + 1)(2S_N + 1)$ matrix element by a nuclear response function $F_{ij}^{NN'}(q^2, v^2)$ [65, 68, 75]. We obtain

$$\overline{|\mathcal{M}_T|^2} = \frac{1}{2S_V + 1} \frac{1}{2S_T + 1} \sum_N \sum_{s',s} \sum_{r',r} |\mathcal{M}_N|^2 = \frac{m_T^2}{m_N^2} \sum_N \sum_{i,j} c_i^N c_j^{N'} F_{ij}^{NN'}(q^2, v^2). \quad (53)$$

The nuclear response functions account for the coherent enhancement of the cross section at low exchanged momentum and are different for different NR interactions. Moreover, they depend on the kinematic variables q^2 and v^2 , where v is the DM velocity. For convenience, we report here the relevant

expressions:

$$\begin{aligned}
F_{1,1}^{N'N}(M, q^2, v^2) &= F_M^{N'N} = \mathcal{N}_{N'} \mathcal{N}_N F_{\text{SI}}^2(E_R) \quad \text{with } \mathcal{N}_p = Z, \mathcal{N}_n = A - Z, \\
F_{5,5}^{N'N}(M, q^2, v^2) &= \frac{C(S_X)}{4} \frac{1}{q^4} \left[q^2 \left(v^2 - \frac{q^2}{4\mu_T^2} \right) F_M^{N'N} \right], \\
F_{8,8}^{N'N}(M, q^2, v^2) &= \frac{C(S_X)}{4} \left(v^2 - \frac{q^2}{4\mu_T^2} \right) F_M^{N'N}, \\
F_{11,11}^{N'N}(M, q^2, v^2) &= \frac{C(S_X)}{4} q^2 F_M^{N'N}, \\
F_{17,17}^{N'N}(M, q^2, v^2) &= \frac{C(S_X)}{4} q^2 \left(v^2 - \frac{q^2}{4\mu_T^2} \right) F_M^{N'N}, \\
F_{19,19}^{N'N}(M, q^2, v^2) &= \frac{C(S_X)}{4} q^4 F_M^{N'N},
\end{aligned} \tag{54}$$

where the DM spin dependent factor $C(S) = 4S(S+1)/3 = 8/3$ for a spin-1 candidate. No interference arise between different operators. Approximated expressions for $F_M^{N'N}$ are listed for different target nuclei in Ref. [68]. For simplicity, in our analysis we use the Helm form factor $F_{\text{SI}}^2(E_R)$, whose expression can be found in [65, 68, 75]. This approximation does not introduce any large error, since at very low recoil energy (*i.e.* in the most relevant region for direct detection experiments) F_M and F_{SI}^2 give basically the same results.

The differential DM-target scattering cross section in the LAB frame is given by:

$$\frac{d\sigma_T}{dE_R} = \frac{|\overline{\mathcal{M}_T}|^2}{32\pi M^2 m_T v^2}. \tag{55}$$

Finally, we are in the position of giving explicit expressions for the differential detection rate [65, 75]:

$$\frac{dR}{dE_R}(E_R) = \frac{\rho_{\text{DM}}}{32\pi M^3 m_N^2} A^2 \sum_{i,j} c_i c_j \mathcal{F}_{i,j}^{N'N}(M, E_R), \tag{56}$$

where ρ_{DM} is the DM density on Earth and the integrated form factors expressions are given by

$$\mathcal{F}_{i,j}^{N'N}(M, E_R) = \int_{v \geq v_{\min}(E_R)} d^3v \frac{f_{\text{SHM,E}}(\vec{v})}{v} F_{i,j}^{N'N}(M, q^2, v^2) \Big|_{q^2=2m_T E_R}. \tag{57}$$

In the previous equation, we take the velocity distribution $f_{\text{SHM,E}}$ in Earth's frame to be

$$f_{\text{SHM,E}} = \frac{e^{-(v+v_E)^2/v_0^2} - \beta e^{-v_{\text{esc}}^2/v_0^2}}{(v_0\sqrt{\pi})^3 N_{\text{esc}}} \Theta(v_{\text{esc}} - |v + v_E|), \tag{58}$$

with N_{esc} being a normalization factor which goes to one as we send the escape velocity to infinity. The minimum velocity for which we have a direct detection scattering event is $v_{\min}(E_R) = (m_T E_R / 2\mu_{TV}^2)^{1/2}$, with $\mu_{TV} = Mm_T / (M + m_T)$ the DM-target reduced mass. From the practical point of view, we compute the velocity integrals using the expressions presented in Appendix A of [75]. The expected numbers of observed events, computed as a function of the EFT parameters ($\mathcal{C}_i, M_\star, g_\star$)

can be found integrating over the nuclear recoil energy in the range indicated by experiments, after having multiplied eq. (56) by the total exposure:

$$N_{\text{th}} = T_{\text{exp}} M_{\text{exp}} \int_{E_{R_{\text{min}}}}^{E_{R_{\text{max}}}} \frac{dR}{dE_R}(E_R), \quad (59)$$

where T_{exp} is the total time over which the experiment ran and M_{exp} the total mass of the experiment.

References

- [1] M. Cirelli, A. Strumia, and J. Zupan, *Dark Matter*, [arXiv:2406.01705](#).
- [2] J. C. Criado, A. Djouadi, M. Perez-Victoria, and J. Santiago, *A complete effective field theory for dark matter*, *JHEP* **07** (2021) 081, [[arXiv:2104.14443](#)].
- [3] J. de Blas, J. C. Criado, M. Perez-Victoria, and J. Santiago, *Effective description of general extensions of the Standard Model: the complete tree-level dictionary*, *JHEP* **03** (2018) 109, [[arXiv:1711.10391](#)].
- [4] M. Fabbrichesi, E. Gabrielli, and G. Lanfranchi, *The dark photon*, *SpringerBriefs in Physics* 2020 (05, 2020) [[arXiv:2005.01515](#)].
- [5] A. Caputo, A. J. Millar, C. A. J. O’Hare, and E. Vitagliano, *Dark photon limits: A handbook*, *Phys. Rev. D* **104** (2021), no. 9 095029, [[arXiv:2105.04565](#)].
- [6] O. Lebedev, H. M. Lee, and Y. Mambrini, *Vector Higgs-portal dark matter and the invisible Higgs*, *Phys. Lett. B* **707** (2012) 570–576, [[arXiv:1111.4482](#)].
- [7] Y. Farzan and A. R. Akbarieh, *VDM: A model for Vector Dark Matter*, *JCAP* **10** (2012) 026, [[arXiv:1207.4272](#)].
- [8] S. Baek, P. Ko, W.-I. Park, and E. Senaha, *Higgs Portal Vector Dark Matter : Revisited*, *JHEP* **05** (2013) 036, [[arXiv:1212.2131](#)].
- [9] M. Duch, B. Grzadkowski, and M. McGarrie, *A stable Higgs portal with vector dark matter*, *JHEP* **09** (2015) 162, [[arXiv:1506.08805](#)].
- [10] A. DiFranzo, P. J. Fox, and T. M. P. Tait, *Vector Dark Matter through a Radiative Higgs Portal*, *JHEP* **04** (2016) 135, [[arXiv:1512.06853](#)].
- [11] M. Duch, B. Grzadkowski, and D. Huang, *Strongly self-interacting vector dark matter via freeze-in*, *JHEP* **01** (2018) 020, [[arXiv:1710.00320](#)].
- [12] D. Azevedo, M. Duch, B. Grzadkowski, D. Huang, M. Igllicki, and R. Santos, *Testing scalar versus vector dark matter*, *Phys. Rev. D* **99** (2019), no. 1 015017, [[arXiv:1808.01598](#)].
- [13] S. Yaser Ayazi and A. Mohamadnejad, *Conformal vector dark matter and strongly first-order electroweak phase transition*, *JHEP* **03** (2019) 181, [[arXiv:1901.04168](#)].
- [14] S. Glaus, M. Mühlleitner, J. Müller, S. Patel, and R. Santos, *Electroweak Corrections to Dark Matter Direct Detection in a Vector Dark Matter Model*, *JHEP* **10** (2019) 152, [[arXiv:1908.09249](#)].
- [15] G. Arcadi, A. Djouadi, and M. Kado, *The Higgs-portal for vector dark matter and the effective field theory approach: A reappraisal*, *Phys. Lett. B* **805** (2020) 135427, [[arXiv:2001.10750](#)].

- [16] K. Ghorbani, *Light vector dark matter with scalar mediator and muon $g-2$ anomaly*, *Phys. Rev. D* **104** (2021), no. 11 115008, [[arXiv:2104.13810](#)].
- [17] G. Arcadi, A. Djouadi, and M. Kado, *The Higgs-portal for dark matter: effective field theories versus concrete realizations*, *Eur. Phys. J. C* **81** (2021), no. 7 653, [[arXiv:2101.02507](#)].
- [18] A. Amiri, B. Díaz Sáez, and K. Ghorbani, *(sub)GeV Dark Matter in the $U(1)_X$ Higgs Portal Model*, [arXiv:2209.11723](#).
- [19] M. T. Frandsen, M. E. Thing, M. Heikinheimo, K. Tuominen, and M. Rosenlyst, *Vector dark matter in supercooled Higgs portal models*, *Phys. Rev. D* **108** (2023), no. 1 015033, [[arXiv:2301.00041](#)].
- [20] T. Hambye, *Hidden vector dark matter*, *JHEP* **01** (2009) 028, [[arXiv:0811.0172](#)].
- [21] S. Baek, P. Ko, and W.-I. Park, *Hidden sector monopole, vector dark matter and dark radiation with Higgs portal*, *JCAP* **10** (2014) 067, [[arXiv:1311.1035](#)].
- [22] C.-H. Chen and T. Nomura, *Searching for vector dark matter via Higgs portal at the LHC*, *Phys. Rev. D* **93** (2016), no. 7 074019, [[arXiv:1507.00886](#)].
- [23] J. S. Kim, O. Lebedev, and D. Schmeier, *Higgsophilic gauge bosons and monojets at the LHC*, *JHEP* **11** (2015) 128, [[arXiv:1507.08673](#)].
- [24] C.-H. Chen and T. Nomura, *$SU(2)_X$ vector DM and Galactic Center gamma-ray excess*, *Phys. Lett. B* **746** (2015) 351–358, [[arXiv:1501.07413](#)].
- [25] V. V. Khoze and A. D. Plascencia, *Dark Matter and Leptogenesis Linked by Classical Scale Invariance*, *JHEP* **11** (2016) 025, [[arXiv:1605.06834](#)].
- [26] B. Barman, S. Bhattacharya, S. K. Patra, and J. Chakraborty, *Non-Abelian Vector Boson Dark Matter, its Unified Route and signatures at the LHC*, *JCAP* **12** (2017) 021, [[arXiv:1704.04945](#)].
- [27] B. Barman, S. Bhattacharya, and M. Zakeri, *Multipartite Dark Matter in $SU(2)_N$ extension of Standard Model and signatures at the LHC*, *JCAP* **09** (2018) 023, [[arXiv:1806.01129](#)].
- [28] I. Chaffey and P. Tanedo, *Vector self-interacting dark matter*, *Phys. Rev. D* **101** (2020), no. 7 075005, [[arXiv:1907.10217](#)].
- [29] T. Nomura, H. Okada, and S. Yun, *Vector dark matter from a gauged $SU(2)$ symmetry*, *JHEP* **06** (2021) 122, [[arXiv:2012.11377](#)].
- [30] N. Baouche, A. Ahriche, G. Faisel, and S. Nasri, *Phenomenology of the hidden $SU(2)$ vector dark matter model*, *Phys. Rev. D* **104** (2021), no. 7 075022, [[arXiv:2105.14387](#)].
- [31] Z. Hu, C. Cai, Y.-L. Tang, Z.-H. Yu, and H.-H. Zhang, *Vector dark matter from split $SU(2)$ gauge bosons*, *JHEP* **07** (2021) 089, [[arXiv:2103.00220](#)].
- [32] Z. Zhang, C. Cai, and H.-H. Zhang, *Hidden $SU(2)_D$ vector dark matter with a scalar septuplet*, *Phys. Rev. D* **106** (2022), no. 11 115022, [[arXiv:2209.01980](#)].
- [33] A. Belyaev, A. Deandrea, S. Moretti, L. Panizzi, D. A. Ross, and N. Thongyoi, *A fermionic portal to vector dark matter from a new gauge sector*, [arXiv:2204.03510](#).
- [34] T. Hambye and M. H. G. Tytgat, *Confined hidden vector dark matter*, *Phys. Lett. B* **683** (2010) 39–41, [[arXiv:0907.1007](#)].

- [35] A. Karam and K. Tamvakis, *Dark Matter from a Classically Scale-Invariant $SU(3)_X$* , *Phys. Rev. D* **94** (2016), no. 5 055004, [[arXiv:1607.01001](#)].
- [36] P. Ko and Y. Tang, *Residual Non-Abelian Dark Matter and Dark Radiation*, *Phys. Lett. B* **768** (2017) 12–17, [[arXiv:1609.02307](#)].
- [37] G. Arcadi, C. Gross, O. Lebedev, Y. Mambrini, S. Pokorski, and T. Toma, *Multicomponent Dark Matter from Gauge Symmetry*, *JHEP* **12** (2016) 081, [[arXiv:1611.00365](#)].
- [38] C. Gross, O. Lebedev, and Y. Mambrini, *Non-Abelian gauge fields as dark matter*, *JHEP* **08** (2015) 158, [[arXiv:1505.07480](#)].
- [39] S. Di Chiara and K. Tuominen, *A minimal model for $SU(N)$ vector dark matter*, *JHEP* **11** (2015) 188, [[arXiv:1506.03285](#)].
- [40] M. Frigerio, N. Grimbaum-Yamamoto, and T. Hambye, *Dark matter from the centre of $SU(N)$* , [arXiv:2212.11918](#).
- [41] B. D. Sáez, F. Rojas-Abatte, and A. R. Zerwekh, *Dark Matter from a Vector Field in the Fundamental Representation of $SU(2)_L$* , *Phys. Rev. D* **99** (2019), no. 7 075026, [[arXiv:1810.06375](#)].
- [42] T. Abe, M. Fujiwara, J. Hisano, and K. Matsushita, *A model of electroweakly interacting non-abelian vector dark matter*, *JHEP* **07** (2020) 136, [[arXiv:2004.00884](#)].
- [43] D. Barducci, E. Bertuzzo, G. Grilli di Cortona, and G. M. Salla, *Dark photon bounds in the dark EFT*, *JHEP* **12** (2021) 081, [[arXiv:2109.04852](#)].
- [44] G. D. Kribs, G. Lee, and A. Martin, *Effective field theory of Stückelberg vector bosons*, *Phys. Rev. D* **106** (2022), no. 5 055020, [[arXiv:2204.01755](#)].
- [45] J. Hisano, K. Ishiwata, N. Nagata, and M. Yamanaka, *Direct Detection of Vector Dark Matter*, *Prog. Theor. Phys.* **126** (2011) 435–456, [[arXiv:1012.5455](#)].
- [46] Z.-H. Yu, J.-M. Zheng, X.-J. Bi, Z. Li, D.-X. Yao, and H.-H. Zhang, *Constraining the interaction strength between dark matter and visible matter: II. scalar, vector and spin-3/2 dark matter*, *Nucl. Phys. B* **860** (2012) 115–151, [[arXiv:1112.6052](#)].
- [47] J. Kumar, D. Marfatia, and D. Yaylali, *Vector dark matter at the LHC*, *Phys. Rev. D* **92** (2015), no. 9 095027, [[arXiv:1508.04466](#)].
- [48] A. Belyaev, L. Panizzi, A. Pukhov, and M. Thomas, *Dark Matter characterization at the LHC in the Effective Field Theory approach*, *JHEP* **04** (2017) 110, [[arXiv:1610.07545](#)].
- [49] A. Belyaev, E. Bertuzzo, C. Caniu Barros, O. Eboli, G. Grilli Di Cortona, F. Iocco, and A. Pukhov, *Interplay of the LHC and non-LHC Dark Matter searches in the Effective Field Theory approach*, *Phys. Rev. D* **99** (2019), no. 1 015006, [[arXiv:1807.03817](#)].
- [50] J. Aebischer, W. Altmannshofer, E. E. Jenkins, and A. V. Manohar, *Dark matter effective field theory and an application to vector dark matter*, *JHEP* **06** (2022) 086, [[arXiv:2202.06968](#)].
- [51] S.-M. Choi, Y. Hochberg, E. Kuflik, H. M. Lee, Y. Mambrini, H. Murayama, and M. Pierre, *Vector SIMP dark matter*, *JHEP* **10** (2017) 162, [[arXiv:1707.01434](#)].
- [52] K. Kaneta, H.-S. Lee, and S. Yun, *Dark photon relic dark matter production through the dark axion portal*, *CTPU-17-15* (04, 2017) [[arXiv:1704.07542](#)].

- [53] S. Fraser, E. Ma, and M. Zakeri, *SU(2)_N model of vector dark matter with a leptonic connection*, *Int. J. Mod. Phys. A* **30** (2015), no. 03 1550018, [[arXiv:1409.1162](#)].
- [54] P. Ko, T. Nomura, and H. Okada, *Dark matter physics in dark SU(2) gauge symmetry with non-Abelian kinetic mixing*, *Phys. Rev. D* **103** (2021) 095011, [[arXiv:2007.08153](#)].
- [55] C. Cai and H.-H. Zhang, *Vector dark matter production from catalyzed annihilation*, *JHEP* **01** (2022) 099, [[arXiv:2107.13475](#)].
- [56] H. Zhou, *Quasi-degenerate dark photon and dark matter*, [arXiv:2209.08843](#).
- [57] C.-W. Chiang, T. Nomura, and J. Tandean, *Nonabelian Dark Matter with Resonant Annihilation*, *JHEP* **01** (2014) 183, [[arXiv:1306.0882](#)].
- [58] H. Davoudiasl and I. M. Lewis, *Dark Matter from Hidden Forces*, *Phys. Rev. D* **89** (2014), no. 5 055026, [[arXiv:1309.6640](#)].
- [59] R. Catena and T. R. Gray, *Spin-1 Thermal Targets for Dark Matter Searches at Beam Dump and Fixed Target Experiments*, [arXiv:2307.02207](#).
- [60] V. V. Khoze and G. Ro, *Dark matter monopoles, vectors and photons*, *IPPP/14/53, DCPT/14/106* (06, 2014) [[arXiv:1406.2291](#)].
- [61] X. Chu, J. Hisano, A. Ibarra, J.-L. Kuo, and J. Pradler, *Multipole vector dark matter below the GeV scale*, *Phys. Rev. D* **108** (2023), no. 1 015029, [[arXiv:2303.13643](#)].
- [62] J. Hisano, A. Ibarra, and R. Nagai, *Direct detection of vector dark matter through electromagnetic multipoles*, *JCAP* **10** (2020) 015, [[arXiv:2007.03216](#)].
- [63] O. Antipin, M. Redi, A. Strumia, and E. Vigiani, *Accidental Composite Dark Matter*, *JHEP* **07** (2015) 039, [[arXiv:1503.08749](#)].
- [64] G. D'Ambrosio, G. F. Giudice, G. Isidori, and A. Strumia, *Minimal flavor violation: An Effective field theory approach*, *Nucl. Phys. B* **645** (2002) 155–187, [[hep-ph/0207036](#)].
- [65] E. Del Nobile, *The Theory of Direct Dark Matter Detection: A Guide to Computations*, [arXiv:2104.12785](#).
- [66] E. D. Nobile, M. Cirelli, and P. Panci, *Tools for model-independent bounds in direct dark matter searches*, *SACLAY-T13/022; CP3-Origins-2013-014 DNRFP90; DIAS-2013-14* (07, 2013) [[arXiv:1307.5955](#)].
- [67] J. Fan, M. Reece, and L.-T. Wang, *Non-relativistic effective theory of dark matter direct detection*, *JCAP* **11** (2010) 042, [[arXiv:1008.1591](#)].
- [68] A. L. Fitzpatrick, W. Haxton, E. Katz, N. Lubbers, and Y. Xu, *The Effective Field Theory of Dark Matter Direct Detection*, *JCAP* **02** (2013) 004, [[arXiv:1203.3542](#)].
- [69] J. B. Dent, L. M. Krauss, J. L. Newstead, and S. Sabharwal, *General analysis of direct dark matter detection: From microphysics to observational signatures*, *Phys. Rev. D* **92** (2015), no. 6 063515, [[arXiv:1505.03117](#)].
- [70] R. Catena, K. Fridell, and M. B. Krauss, *Non-relativistic Effective Interactions of Spin 1 Dark Matter*, *JHEP* **08** (2019) 030, [[arXiv:1907.02910](#)].
- [71] P. Gondolo, S. Kang, S. Scopel, and G. Tomar, *Effective theory of nuclear scattering for a WIMP of arbitrary spin*, *Phys. Rev. D* **104** (2021), no. 6 063017, [[arXiv:2008.05120](#)].

- [72] **Particle Data Group** Collaboration, R. L. Workman and Others, *Review of Particle Physics*, *PTEP* **2022** (2022) 083C01.
- [73] **LZ** Collaboration, J. Aalbers et al., *First Dark Matter Search Results from the LUX-ZEPLIN (LZ) Experiment*, *Phys. Rev. Lett.* **131** (2023), no. 4 041002, [[arXiv:2207.03764](#)].
- [74] S.-M. Choi, H. M. Lee, Y. Mambrini, and M. Pierre, *Vector SIMP dark matter with approximate custodial symmetry*, *JHEP* **07** (2019) 049, [[arXiv:1904.04109](#)].
- [75] M. Cirelli, E. Del Nobile, and P. Panci, *Tools for model-independent bounds in direct dark matter searches*, *JCAP* **10** (2013) 019, [[arXiv:1307.5955](#)].